National Research University Higher School of Economics

As a manuscript

Garashchuk Ivan Ruslanovich

Nonlinear dynamics and hyperchaos in two biophysical models of coupled nonlinear oscillators

Dissertation summary
for the purpose of obtaining academic degree
Doctor of Philosophy in Applied Mathematics

Academic supervisor:
Candidate of Sciences in Physics and Mathematics
Sinelshchikov Dmitry Igorevich

Moscow – 2023

Introduction

Relevance

Dynamical systems describe processes with a deterministic law of evolution. They are used for modeling a variety of phenomena in many branches of science, such as physics, chemistry and biology [1].

Depending on the requirements of a specific application and the model's complexity, the governing dynamical system can be studied using either analytical or numerical methods. Regardless of the approach, performing bifurcation analysis, i.e. studying qualitative changes in the system's behavior with variations of the control parameters, is usually of interest. Therefore, during numerical simulations generally the Lyapunov exponents are computed along with evolution of the phase variables, because it allows one to determine the type of dynamics on an attractor [2; 3]. For instance, the presence of a positive Lyapunov exponent in the spectrum can be used as the criterion of chaotic dynamics [4]. Therefore, the charts of dependence of the spectra of the Lyapunov exponents on the control parameters can be used as a tool for bifurcation analysis.

In this work we study two models of coupled nonlinear oscillators that occur in biophysical applications. The first one is the model of two interacting encapsulated gas bubbles in a liquid. It is important, because such bubbles are used in modern medicine as contrast agents during ultrasound examinations for enhanced visualization of certain organs or areas of the circulatory system, as well as in applications related to the targeted drug delivery [5–8].

The acoustic response of the contrast agents is formed by radial oscillations of the bubbles under the influence of the external ultrasound field. Nonlinearity of the oscillations leads to a variety of possible dynamical regimes, such as subharmonic (with the respect to the external filed), quasiperiodic or chaotic. At the same time, the properties of the response, as well as the long-term stability of the contrast agents, depend on the regime of the oscillations. For instance, subharmonic and chaotic regimes are considered beneficial for ultrasound visualization problems, because the spectrum of the pressure field radiated by the bubbles drastically differs from the spectrum of the acoustic waves emitted by the surrounding tissues, oscillations of which are close to linear [5; 9; 10]. Hyperchaotic regimes of bubbles oscillations are also beneficial for effective detection of the contrast agents, but they can lead to faster shell rupture and dissolution of the bubbles. On the other hand, this property can be useful in some targeted drug delivery problems, when a quick controlled shell disruption is desirable.

Thus, the dynamics of the contrast oscillations are closely related to their acoustic properties. The models of their behavior are based on the Rayleigh-Plesset equation, which was derived to describe spherical gas bubbles in an incompressible liquid [11]. To correctly model the contrast agents, one has to take into account their viscoelastic shell. A number of different approaches to describe the shell exists. Applicability of each of them to specific types of contrast agents depends on the material and thickness of the particular shell, as well as the necessity of taking into account its rupture during large-amplitude oscillations, etc. (see discussion in [9], and also [5; 10; 12; 13]). In this work we describe the SonoVue contrast agents with a thin lipid shell using the de-Jong model [12; 14]. In addition we take into account liquid's compressibility using the Keller-Miksis approach [15]. Because there is an ensemble of contrast agents injected

into the blood flow, they interact via the acoustic waves radiated by each of them. The influence of such interaction is described by the Bjerknes force [16], and can significantly impact the dynamics of bubbles oscillations within the cluster [16–20].

The second model we consider here is the model of coupled neurons. The excitability of neurons plays crucial role in signal transmission in the nervous system. The electrical mechanisms of excitation of a neuronal cell and generation of the action potential are well described by the Hodgkin-Huxley model [21]. The Hindmarsh-Rose system, derived within the Hodgkin-Huxley formalism, was proposed in [22] to reproduce the bursting firing patterns of the neuronal membrane potential, observed in experiments [22]. It is widely used for describing excitable cells, in which such patterns play an important biological role [23]. In a human body such cells form networks of interacting elements, and modeling their behavior has applied interest. Moreover, according to modern studies, some specific dynamical regimes, such as synchronous periodic firing in certain groups of neurons is associated with pathological behavior [24], and finding the areas of stability of such regimes in the parameters space can be important.

Moreover, studying such phenomena as hyperchaotic dynamics and synchronization, appearing in these models, is relevant from the dynamical systems point of view. Dynamics on an attractor is called hyperchaotic if hyperbolic instabilities of dimension two or higher are present. Numerically this is expressed by positiveness of two or more Lyapunov exponents. Recall that divergence of flux of a smooth dissipative dynamical system must be negative on any attractor. It corresponds to the sum of Lyapunov exponents associated with the same attractor. Therefore, hyperchaotic dynamics can be observed only in four- or higher-dimensional systems.

The first example of hyperchaotic attractor was found in the four-dimensional Rössler system [25]. Later, presence of hyperchaotic regimes was observed in a variety of dynamical systems (see, e.g. [26–28]). Experimental confirmation of hyperchaotic behavior in physical systems was obtained in works on dynamics in electrical circuits [29], laser systems with nuclear magnetic resonance [30] and p-Ge semiconductors [31]. However, bifurcation scenarios of emergence of hypoerchaotic strange attractors in multidimensional systems are not sufficiently studied [32].

Another interesting effect, occurring in the considered models, is synchronization of oscillations in systems of coupled nonlinear oscillators. Synchronous regimes have qualitative differences from the asynchronous ones from perspective of the dynamics and as well as the applications [33]. The phenomenon of the destruction of synchronization observed in the considered models, and it is interesting to study from the dynamical systems perspective. Moreover, in some cases it is related to the emergence of hyperchaotic dynamics.

Current state of the research topic

In the area of modeling the oscillations of the microbubble contrast agents, a number of studies on dynamics of individual bubbles without interaction exists. Work [34] is dedicated to the detailed study of bifurcation structure of the model of a non-shelled gas bubble. More complex models of dynamics of individual contrast agents in a shell were considered in [10; 35; 36]. However, in [36] the authors did not correctly take into account multistability of the system. There are also several studies dedicated to dynamics of two or more interacting contrast

agents [17; 20; 37]. However, in work [17] bubbles without shells were considered, while in [20; 37] an incorrect shell model was used (see discussion in [9]). The authors of [38] considered a large cluster of contrast agents, while using a technique for dimensionality reduction, allowing for efficient finding of synchronous regimes of the bubbles oscillations. However, as we show here, synchronous dynamical regimes can be transversally unstable or unstable with respect to symmetry breaking perturbations, while multistability also plays a substantial role in dynamics of several interacting contrast agents. On the other hand, the case of two bubbles with correct accounting for both the shell and the interaction has not been considered earlier. It is important, because studying the dynamics in such system is necessary for understanding the oscillations of contrast agents in a cluster. It also allows one to examine the influence of the coupling strength on the dynamical regimes and synchronization of the oscillations. Therefore, we propose a model of two interacting contrast agents encapsulated in shells and study the dynamics in it.

Now let us consider modeling of the behavior of individual and interacting neurons. The dynamics in the Hindmarsh-Rose system describing a single neuron has been thoroughly studied in [39–42]. A number of works is dedicated to studying the behavior in ensembles of two or more neurons [43–45] and effects related to synchronization in large networks [46; 47]. However, dynamics in small ensembles of interacting neurons is not well understood, especially stability of the synchronous attractors, corresponding to the regimes of a single neuron. Besides that, new asynchronous attractors emerging in small ensembles are also of interest. Thus, we study the dynamics and synchronization in the minimal ensemble of two coupled neurons. We also consider mechanisms of its excitability and model its excitation by signals from an external neuron.

As far as the hyperchaotic attractors are concerned, examples of them were known for a while [25; 48]. Despite that, the mechanisms of their emergence have not been studied until recently. The exception is systems of weakly coupled oscillators, in which appearance of hyperchaotic dynamics was explained by emergence of chaotic attractors in each of the subsystems [49; 50]. In works [51; 52] the authors mentioned that for the transition from chaotic dynamics to hyperchaotic, inclusion of saddle orbits with two-dimensional unstable manifolds into the attractor is necessary. However, bifurcation mechanisms of appearance of such trajectories were not explained. Besides that, the scenarios of emergence of hyperchaotic attractors in Hénon-type maps were studied in work [53]. Hyperchaotic nature of the discrete Shilnikov attractors was also noted in [54; 55]. Therefore, it is important to study the underlying bifurcation mechanism, leading to the emergence of hyperchaotic dynamics in the physical models of coupled nonlinear oscillators, considered in this work.

Aim and problems of the work

The aim of this work is to study the dynamics in two applied systems of coupled nonlinear oscillators and to uncover new bifurcation scenarios of emergence of hyperchaotic oscillations. To achieve this aim the following problems were solved:

1. Proposition of a mathematical model of two gas bubbles taking into account their shells, liquid's viscosity and compressibility, their interaction via the Bjerknes force and the external pressure field.

2. Development of a modification of the algorithm of computing the Lyapunov exponents allowing for detailed studying of dynamics when destruction of synchronization occurs. Implementation a software package for numerical studying of the considered models.

3. Studying dynamics in the model of two interacting microbubble contrast agents taking multistability into account. Proposing new scenarios explaining onset of hyperchaotic attractors in the model.

4. Identifying domains in the parameters space of the model of two contrast agents, in which synchronization of oscillations takes place. Identification the scenarios of emergence of synchronous and asynchronous dynamical regimes. Explaining the destruction of synchronization occurring in the model.

5. Studying dynamics in the model of two coupled neurons and analyzing transversal stability of the synchronous invariant sets.

6. Explaining the underlying mechanisms of excitability of the group of two coupled neurons. Modeling of excitation of such group by external signals generated by a separate neuron.

Research methods

We use a combination of numerical and analytical methods to solve these problems. We utilize analytical methods to look for stationary points and carry out the linear stability analysis.

We apply adaptive methods suitable for integration of stiff systems for finding of individual trajectories of the dynamical systems. We use the method of inheriting initial conditions, based on the concept of continuity by a parameter, to get initial conditions with changing control parameters. This approach is necessary due to inherent multistability of the considered systems.

In order to establish the types of dynamics we use a combination of methods of constructing the Poincaré maps and calculating the spectrum of Lyapunov exponents. We construct charts of the spectra of Lyapunov exponents by the control parameters to analyze bifurcations. To determine transversal stability of a synchronous regime we calculate the largest transversal Lyapunov exponent. We also implement a method of separate computing of the spectrum of Lyapunov exponents for synchronous and asynchronous components of the trajectory to study the dynamics during the destruction of synchronization and loss of transervsal stability in more details. In order to speed up the calculations of the charts of Lyapunov exponents we utilize the methods of parallel computing. For spectral analysis of the numerical solutions we use the fast Fourier transform.

Scientific novelty

- We have proposed a mathematical model describing dynamics of two gas bubbles in shells interacting via the Bjerknes force. We have constructed one- and two-dimensional charts of the regimes of dynamics and studied the bifurcation scenarios of transitions between various types of dynamical regimes.

- We have proposed a scenario of emergence of hyperchaotic attractors in systems of coupled oscillators with external influence, accompanied by the secondary Neimark-Sacker bifurcation and occurrence of a homoclinic Shilnikov attractor.
- We have proposed a scenario of emergence of hyperchaotic attractors in systems of coupled oscillators with external influence, associated with destruction of synchronization via the bubbling transition.
- We have found new asynchronous regimes in the model describing two interacting neurons and established areas of stability of synchronous regimes. We have described mechanisms of excitability of such system and presented the results of modeling of its excitation by a neuronal signal.

Theoretical significance

Despite the fact that numerous examples of hyperchaotic attractors are known, including those in applied models, the bifurcation mechanisms of emergence of two-dimensional instabilities are explained only in specific cases. Here we propose two new scenarios of appearance of hyperchaotic dynamics in wide class of systems of coupled oscillators with external force. The proposed explanation of the bifurcation mechanisms is fairly universal, and implementations of these scenarios have been found in other systems. We have also shown the connection between some phenomena known in the theory of synchronization with emergence of hyperchaotic dynamics.

Practical significance

There exist quite detailed research regarding the oscillations of individual gas bubbles. Despite that, the dynamics in a cluster of contrast agents was considered only in specific cases, and there are practically no detailed studies of dynamics in small clusters with a correct shell model. Here we propose a model of two interacting contrast agents encapsulated in shells, which has not been studied before. We study the dynamics in the model in details taking multistability into account. We have found new regimes of dynamics, not observed before in models of contrast agents. We have constructed charts of the dynamical regimes, showing the relation between the amplitude of the external pressure field and the distance between the bubbles with the regimes of oscillations.

Within the framework of the models of connected neurons, we study the dynamics in a fully-connected group of two elements. We consider stability of the synchronous regimes, and emergence of asynchronous dynamics. We study the mechanisms responsible for excitability of such system and model its excitation by external signals. We use an external neuron as the generator of excitatory signals natural for neuronal systems.

Provisions for defense

1. We have proposed a mathematical model of two coupled gas bubbles taking into account their shells. Within its framework, we have built one- and two-dimensional charts of

the dynamical regimes in a physically relevant area of the control parameters, taking multistability into account. We have established areas in the parameter space, where synchronous oscillations exist. We have described bifurcation scenarios of emergence of regular, chaotic and hyperchaotic dynamics.

2. We have proposed the scenario of emergence of hyperchaotic dynamics, key steps of which are the secondary Neimark-Sacker bifurcation and the appearance of the homoclinic Shilnikov attractor with inclusion of saddle-focus orbits with two-dimensional unstable manifold into the chaotic attractor. We have confirmed the implementation of this scenario in the model of interacting microbubble contrast agents numerically.

3. We have proposed the scenario of appearance of a hyperchaotic attractor based on the destruction of synchronization. We have established that the underlying mechanism of emergence of the transversally unstable areas within a synchronous attractor is the bifurcation cascade known as the bubbling transition. Utilizing the developed modifications of the algorithm of computing the spectrum of Lyapunov exponents, we have numerically confirmed the implementations of this scenario in the model of interacting microbubble contrast agents.

4. Within the framework of the model of two coupled neurons, described by the Hindmarsh-Rose system, we have constructed one-dimensional charts of the dynamical regimes and described the firing patterns. We have established the areas of transversal stability of the synchronous regimes and explained the scenario of emergence of the asynchronous chaotic attractor. We have found the areas of bistability. We studied the bifurcation mechanisms responsible for the excitability of this system, and have proposed a mode of its excitation by a signal, generated by an external neuron. We have constructed charts of excitation of the system by various signals in the areas of stability of the synchronous equilibrium.

Reliability of the results

Reliability of the results of mathematical modeling is confirmed by careful testing of numerical algorithms implemented withing the software package on the known data, results obtained with the help of other software systems and analytical solutions. The main results of the research were presented on international scientific conferences and published in peer-reviewed journals. All the provisions for defense are published in scientific journals indexed in scientific databases Web of Science or Scopus. Three papers were published in journals in the Q1 quartile, and two papers were published in journals in the Q3 quartile.

Approbation of the results

The main results of this work were presented on the following international scientific conferences:

1. Topological methods in dynamics and related topics, “Nonlinear dynamics and typical bifurcations in the model of three coupled ultrasound contrast agents”, May 2022.

2. Shilnikov Workshop, «Asynchronous chaos and bifurcations in a model of two coupled Hindmarsh-Rose neurons», December 2021.

3. SIAM Conference on Applications of Dynamical Systems, "Hyperchaos and Synchronization in a Model of Two Interacting Encapsulated Microbubbles", May 2021.

4. International Conference 'Topological Methods in Dynamics and Related Topics. Shilnikov Workshop.'. "Synchronization and symmetry breaking in a model of two interacting ultrasound contrast agents", December 2020.

5. International Conference 'Topological Methods in Dynamics and Related Topics. Shilnikov Workshop.'. "Symmetry breaking in a system of two coupled microbubble contrast agents", December 2019.

6. International Conference 'Shilnikov Workshop'. "Multistability and Hyperchaos in the Dynamics of Two Coupled Contrast Agents", December 2018.

The results obtained during the research were used in the following scientific projects:

- 2020-2022. RFBR Grant 20-31-90122 for PhD students "Hyperchaos and mechanisms of its emergence, multistability and synchronization in models of interacting neurons".
- 2019-2022. Grant of Ministry of Science and Higher Education of the Russian Federation agreement № 075-15-2019-1931.
- RSF Grant 19-71-10048 "Theory of hyperchaos and its applications to problems of biomedicine".

List of papers submitted for the thesis defense

The main results of the dissertation research were published in 5 papers, indexed in Scopus:

[**1***] Garashchuk I.R., Sinelshchikov D.I, Kazakov A.O., Kudryashov N.A., *Hyperchaos and multistability in the model of two interacting microbubble contrast agents*, Chaos (2019), **29**, 1199–1213.

[**2***] Garashchuk I.R., Sinelshchikov D.I, Kazakov A.O., *Synchronous oscillations and symmetry breaking in a model of two interacting ultrasound contrast agents*, Nonlinear Dynamics (2020), **101**, 1199–1213.

[**3***] Garashchuk I.R., Sinelshchikov D.I, *Bubbling transition as a mechanism of destruction of synchronous oscillations of identical microbubble contrast agents*, Chaos (2021), **31**, 023130.

[**4***] Garashchuk I.R., *Asynchronous Chaos and Bifurcations in a Model of Two Coupled Identical Hindmarsh–Rose Neurons*, Russian Journal of Nonlinear Dynamics (2021), **17(3)**, 307-320.

[**5***] Garashchuk I.R., . Sinelshchikov D.I, *Excitation of a Group of Two Hindmarsh–Rose Neurons with a Neuron-Generated Signal*, Russian Journal of Nonlinear Dynamics (2023), **19(1)**, 19-34.

1 Summary of the work: main results

1.1 Main concepts and research methods

Let us consider a smooth dynamical system with the right-hand side depending on the control parameters:

$$\dot{x} = f(x, a), \tag{1}$$

where $x = (x_1, \ldots, x_n)$ are the phase variables defined on a certain domain $D \subseteq \mathbb{R}^n$, $f(x) = (f_1, \ldots, f_n)$, $f_1, \ldots, f_n \in C^r(D)$, $r > 1$, and $a \in \mathbb{R}^m$ are the m control parameters. Recall that a closed bounded positive-invariant locally attractive set $K \subset D \subseteq \mathbb{R}^n$ is called an attractor of such system [56].

The systems considered here are inherently multistable in physically relevant areas of the control parameters. Therefore we have to use a special procedure for obtaining initial conditions if the control parameters change. Assume we have two (or more) attractors $K_1, K_2, \ldots$ at a certain value of parameters $a = a^{(0)}$. To study the behavior of K_1 with parameters changing to $a = a^{(l)}$, consider homotopy $F_\mu : a^{(0)} \to a^{(l)}, \mu \in [0, 1]$ [57]. In numerical implementation this one-parametric route in the parameter space is represented by a discrete sequence of values $a^{(0)}, a^{(1)}, \ldots, a^{(l)}$. It is insufficient to simply take some fixed point $x_0^{(0)}$ and use it as initial conditions on each parameter step, assuming the trajectory would converge to K_1 after the transient process, because at a certain value of a along the path, $x_0^{(0)}$ can occur in the basin of attraction of K_2. Assume $x_0^{(0)}$ belongs to the basin of K_1 at $a = a^{(j-1)}$, and to the basin of K_2 at $a = a^{(j)}$. Then, after the step from $a^{(j-1)}$ to $a = a^{(j)}$ will be accompanied by a sharp change in systems dynamics associated with the multistable leap, despite absence of any bifurcations of attractor K_1 at this point. Therefore, we implement the algorithm of inheriting the initial conditions, based on the idea of continuation by a parameter. On each parameter step, we choose the last value of $x(t)$ on the attractor K_1 as the initial condition x_0^{i+1} used at the next value $a^{(i+1)}$. If the step of the parameter a is sufficiently small, such algorithm allows us to avoid multistable leaps, associated with the initial point crossing the separatrix between basins of the attractors.

The main tool we use to numerically determine the type of dynamics on an attractor is the spectrum of Lyapunov exponents. They characterize the growth of small perturbations in linear approximation [3]. Let $x(t) \subset \mathbb{R}^n$ be a smooth trajectory of dynamical system (1) starting from the initial point $x(0) = x_0 \in \mathbb{R}^n$. Then the perturbed orbit can be represented as $\tilde{x}(t) = x(t) + \delta x(t)$, where $\delta x(t) : \forall t > 0, \|\delta x(t)\| \ll 1$ describes the evolution of the small perturbation. The initial conditions for this perturbed trajectory are $\tilde{x}(0) = x_0 + \delta x_0, \delta x_0 \in \mathbb{R}^n : \|\delta x_0\| \ll 1$. Then, equation (1) for the perturbed orbit can be written as $\dot{\tilde{x}}(t) = f(x + \delta x)$. Expanding the right hand side of it into the Taylor series, we obtain the following equation for the evolution of the small perturbation in linear approximation:

$$\dot{\delta x}(t) = J\delta x, \tag{2}$$

where $J = \frac{\partial f_i(x)}{\partial x_j}, i = \overline{1 \ldots n}, j = \overline{1 \ldots n}$ is the Jacobi matrix on the unperturbed trajectory $x(t)$.

The Lyapunov exponents are defined as the upper limit

$$\Lambda_{\delta x(t)} = \overline{\lim_{T\to+\infty}} \frac{\ln\|\delta x(T)/\delta x_0\|}{T}, T \in \mathbb{R}, T > 0. \tag{3}$$

Notice that system (2) has n linearly independent solutions. They correspond to n exponents in the spectrum, defined by the limit (3): $(\lambda_1, \ldots, \lambda_n), \lambda_1 \geq \lambda_2 \geq \ldots \geq \lambda_n$.

Usually, an orthonormal basis is chosen to initialize the perturbation vectors $\{\delta x_i^0\}_{i=1}^n$, $\|\delta x_i^0\| = \varepsilon$. Their norm ε is chosen according to the characteristic scale of processes in a specific dynamical system. However, when calculating limits (3) increasing time leads to growth of the vectors norms and violation of their orthogonality. Thus, conditions for applying the linear approximation are no longer met. Therefore, it is necessary reorthogonalize and normalize the set of the perturbation vectors. Consider $t = T$ and a nonorthogonal set of vectors $\{\delta x_i(T)\}_{i=1}^n$. Writing them column-wise in a matrix $A(T)$, we can apply decomposition $A(T) = Q(T)R(T)$ [58], where $Q(T)$ is an orthogonal matrix, and $R(T)$ is an upper triangular matrix with positive elements on the main diagonal. Then, the elements on the main diagonal of the matrix equal to the norms of the perturbation vectors $R(T)$: $R_{ii}(T) = \|\delta x_i(T)\|$, while columns of $Q(T)$ represent the new ortonormal basis. We use this basis to initialize the new set of the perturbations vectors on the next step $\delta x_i^0 = Q_{\cdot,i}$. Thus, repeating this procedure M times we get the following expression for the Lyapunov exponents:

$$\lambda_i = \frac{1}{MT} \sum_{k=1}^{M} \ln \frac{\|R_{ii}(kT)\|}{\epsilon}.$$

It is known as the Benettin algorithm [59]. The results of the calculations along a typical trajectory on an attractor for sufficiently long time converge to the values of the Lyapunov exponents that can be attributed to the attractor itself with probability approaching one [59; 60].

Note that any attractor of a dynamical system, except a stable equilibrium, contains a zero Lyapunov exponent within its spectrum. It corresponds to the translations along the attractor. The sum of Lyapunov exponents equals to the average divergence of the phase flux, and thus it is negative for any attractor of a dissipative dynamical system. The presence of a positive Lyapunov exponent in the spectrum indicates existence of instabilities that lead to divergence of close trajectories on the attractor, i.e. chaotic dynamics. In three-dimensional space an attractor can have the following signatures of the Lyapunov exponents:

- $< -, -, - >$ for a stable equilibrium;
- $< 0, -, - >$ for a stable limit cycle;
- $< 0, 0, - >$ for a quasiperiodic attractor;
- $< +, 0, - >$ for a strange chaotic attractor.

If the dimension is increased to $n = 4$, the signature $< +, +, 0, - >$ becomes possible. In the systems of a higher dimension $n > 4$, up to $n - 2$ Lyapunov exponents can be positive. An attractor characterized by two or more positive Lyapunov exponents is called *hyperchaotic*.

The one-to-one relationship between the signature of the spectrum of Lyapunov exponents and the type of dynamics on the attractor makes it possible to use the Lyapunov exponents to construct charts of the dynamical regimes of the considered systems.

In order to determine the transversal stability of a synchronous invariant set we use the largest transversal Lyapunov exponent [33]. Let us consider a system of coupled oscillators

$$\begin{aligned} \dot{x} &= f(x) + \alpha g(y), \\ \dot{y} &= f(y) + \alpha g(x), \end{aligned} \tag{4}$$

where $x \in \mathbb{R}^n, y \in \mathbb{R}^n$. It is symmetrical to the permutation of variables $x \leftrightarrow y$. Note that solutions of the system $\dot{x} = f(x) + \alpha g(x)$ describe trajectories lying inside the manifold $S : x = y$, called the synchronization manifold. A phase trajectory lying in S corresponds to fully synchronous oscillations of both subsystems x and y. Using the following change of variables [33]

$$u = \frac{x+y}{2}, \ v = \frac{x-y}{2},$$

and substituting it into (4), we obtain the system describing the evolution of variables u, v:

$$\begin{aligned} \dot{u} &= \tfrac{1}{2}\left(f(u+v) + f(u-v)\right) + \tfrac{\alpha}{2}\left(g(u-v) + g(u+v)\right), \\ \dot{v} &= \tfrac{1}{2}\left(f(u+v) - f(u-v)\right) + \tfrac{\alpha}{2}\left(g(u-v) - g(u+v)\right). \end{aligned} \tag{5}$$

The variables in (5) have the following meaning: u characterizes the evolution of the phase variables in the direction along S, and v – in the transversal one. The corresponding linear approximation for the perturbation vectors δu, δv looks as follows:

$$\begin{aligned} \dot{\delta u} &= (J_f + \alpha J_g)\delta u, \\ \dot{\delta v} &= (J_f - \alpha J_g)\delta v. \end{aligned} \tag{6}$$

The growth of the solutions of (6) is described by the largest Lyapunov exponents λ_u, λ_v. λ_u characterizes the evolution of perturbations lying inside the synchronization manifold, while λ_v describes the behavior of perturbations along the direction transversal to the synchronization manifold. Thus λ_v is called the largest transversal Lyapunov exponent [33]. The value $\lambda_v > 0$ corresponds to transversal instability of a synchronous solution, meaning that small perturbations grow along the direction transversal to S. We use the Benettin algorithm applied to systems (5), (6) to calculate the largest transversal Lyapunov exponent.

We also propose a modification to the algorithm of computing the spectrum of the Lyapunov exponents for the systems in the form of (4). If a trajectory on an attractor has both the synchronous and the asynchronous component, we calculate the spectrum of the Lyapunov exponents separately for each of them. Let us denote the spectrum, corresponding to the synchronous component as $(\lambda_i^s)_{i=1}^n$, and to the asynchronous one as $(\lambda_i^{as})_{i=1}^n$. If the orbit of the system was inside S for the time T^s and outside of it for T^{as}, the total time is $T = T^{as} + T^s$. Then, the Lyapunov exponents for each component are related to the corresponding exponents along the whole trajectory in the following way: $\lambda_i^s \cdot T^s + \lambda_i^{as} \cdot T^{as} = \lambda_i \cdot T$. We use this modification to study the dynamics if the bifurcation cascade, known as the bubbling transition [61–63], occurs in the system and leads to destruction of synchronization. This allows us to confirm the presence of two-dimensional instabilities in the saddle asynchronous set even if the

Milnor attractor inside the synchronization manifold is transversally stable, and the dynamics is chaotic with one positive Lyapunov exponent.

1.2 Model of interacting microbubble contrast agents

1.2.1 Main system of equations

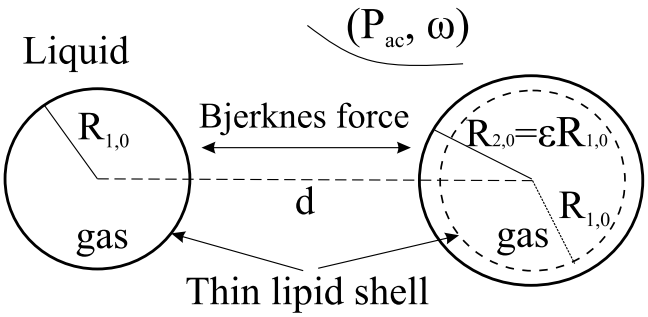

Figure 1: Schematic image of two bubbles in a liquid, oscillating under the influence of the external field, and interacting via the acoustic waves.

if we take into account the visco-elastic shell according to the de-Jong model, compressibility of the liquid according to the Keller-Miksis approach, viscosity at the gas-liquid interface, surface tension and the external ultrasound field

Consider two gas bubbles encapsulated in viscoelastic shells in a liquid, interacting via the Bjerknes force. If we take into account the liquids compressibility and viscosity, surface tension and the influence of the external ultrasound field, the system of equations describing their radial oscillations takes the following form [15–18; 20; 37; 64]:

$$\begin{gathered}\left(1-\frac{\dot{R}_1}{c}\right)R_1\ddot{R}_1+\frac{3}{2}\left(1-\frac{\dot{R}_1}{3c}\right)\dot{R}_1^2=\frac{1}{\rho}\left[1+\frac{\dot{R}_1}{c}+\frac{R_1}{c}\frac{d}{dt}\right]P_1-\frac{d}{dt}\left(\frac{R_2^2\dot{R}_2}{d}\right),\\ \left(1-\frac{\dot{R}_2}{c}\right)R_2\ddot{R}_2+\frac{3}{2}\left(1-\frac{\dot{R}_2}{3c}\right)\dot{R}_2^2=\frac{1}{\rho}\left[1+\frac{\dot{R}_2}{c}+\frac{R_2}{c}\frac{d}{dt}\right]P_2-\frac{d}{dt}\left(\frac{R_1^2\dot{R}_1}{d}\right),\end{gathered}\tag{7}$$

where

$$\begin{gathered}P_i=\left(P_0+\tfrac{2\sigma}{R_{i0}}\right)\left(\tfrac{R_{i0}}{R_i}\right)^{3\gamma}-\tfrac{4\eta_L\dot{R}_i}{R_i}-\tfrac{2\sigma}{R_i}-P_0-4\chi\left(\tfrac{1}{R_{i0}}-\tfrac{1}{R_i}\right)-\\ -4\kappa_S\tfrac{\dot{R}_i}{R_i^2}-P_{ac}\sin(\omega t),\quad i=1,2.\end{gathered}$$

Here t is time, $R_1(t), R_2(t)$ denote radii of each bubble, d is the distance between their centers, P_{stat} denotes the static pressure, P_v – the vapor pressure, $P_0 = P_{\text{stat}} - P_v$, and P_{ac} is the amplitude of the external pressure field with cyclic frequency ω. σ is the surface tension, ρ is the liquids density and η_L – its viscosity, c corresponds to the speed of sound, γ is the polytropic exponent, χ is the elasticity of the shell, while κ_s is its viscosity and R_{i0} is the equilibrium radius of i-th bubble in absence of the external field. Notice that equations (7) can be resolved with respect to the derivatives of the highest order and rewritten in the form of a five-dimensional dynamical system.

For the liquid's parameters, we use experimental values, corresponding to the blood plasma: $P_{stat} = 100$ kPa, $\sigma = 0.0725$ N/m, $\rho = 1000$ kg/m^3, $\eta_L = 0.001$ N s/m^3, $c = 1500$ m/s. The values of the shell parameters and the gas inside are taken with accordance to the experimental results for the SonoVue contrast agents: $P_v = 2.33$ kPa, $\gamma = 4/3$, $\chi = 0.22$ N/m, $\kappa_S = 2.5 \cdot 10^{-9}$ kg/s, $R_{i0} = 1.72$ μm, $i = 1, 2$ [14]. We consider P_{ac}, ω and d as the control parameters.

We perform the numerical calculations in nondimensional variables $r(\tau), u(\tau)$: $R_i = R_0 r_i$, $t = \omega_0^{-1}\tau$, where $\omega_0^2 = 3\kappa P_0/(\rho R_{10}^2) + 2(3\kappa - 1)\sigma/R_{10} + 4\chi/R_{10}$ is the natural frequency of bubbles oscillations in linear approximation. Thus, the nondimensional speeds of the shells take the following form: $u_i = dr_i/d\tau = \dot{R}_i/(R_0\omega_0)$.

1.2.2 Variety of dynamical regimes

In work [1*] we studied the dynamics in system (7) in the following area of the control parameters: $\omega = 2.87$ s^{-1}, $P_{ac} \in [1.142, 1.89]$ MPa, $d/R_0 \in [6, 35]$. We have constructed the two-dimensional chart of the regimes of dynamics in the system. It is presented in fig. 2a with the following color scheme:

- Blue for periodic dynamics. Omitting the zero Lyapunov exponent, the largest Lyapunov exponents have the following signs: $\lambda_1 < 0, \lambda_2 < 0$;
- Green for quasiperiodic dynamics with the largest Lyapunov exponents are $\lambda_1 = 0, \lambda_2 < 0$;
- Yellow for simply chaotic dynamics (strange attractor with one positive Lyapunov exponent). The signs of the largest Lyapunov exponents are: $\lambda_1 > 0, \lambda_2 < 0$;
- Red for hyperchaotic dynamics with the largest Lyapunov exponents are: $\lambda_1 > 0, \lambda_2 > 0$.

We observed both synchronous and asynchronous limit cycles. On the other hand, we found only asynchronous quasiperiodic regimes in this area of the control parameters. Among the chaotic regimes with one positive Lyapunov exponent we observed both synchronous and asynchronous ones. Since the synchronization manfiold in this case is 3-dimensional, the hyperchaotic regimes cannot be synchronous. In fig. 2 we give examples of phase portraits (or Poincaré maps) of the following regimes: (b) hyperchaotic attractor at $d/R_0 = 32, P_{ac} = 1.68$ MPa with largest Lyapunov exponents of $\lambda_1 = 0.0803$, $\lambda_2 = 0.0357$; (c) synchronous chaotic attractor at $d/R_0 = 30, P_{ac} = 1.4$ MPa with $\lambda_1 = 0.0684$, $\lambda_2 = -0.0268$; (d) syncronous 12-periodic limit cycle at $d/R_0 = 28, P_{ac} = 1.3$ MPa with $\lambda_1 = -0.0616$, $\lambda_2 = -0.0733$; (e) hyperchaotic attractor at $d/R_0 = 22, P_{ac} = 1.2$ MPa with $\lambda_1 = 0.0241$, $\lambda_2 = 0.0034$; (f) quasiperiodic oscillations at $d/R_0 = 14.5, P_{ac} = 1.2$ MPa with $\lambda_1 = 0$, $\lambda_2 = -0.0149$; (g) asynchronous 4-periodic limit cycle at $d/R_0 = 10, P_{ac} = 1.2$ MPa with $\lambda_1 = -0.2331$, $\lambda_2 = -0.2343$; (h) synchronous chaotic attractor at $d/R_0 = 10, P_{ac} = 1.6$ MPa with $\lambda_1 = 0.0802$, $\lambda_2 = -0.0826$; (i) synchronous 2-periodic limit cycle at $d/R_0 = 6.75, P_{ac} = 1.7$ MPa with $\lambda_1 = -0.1437$, $\lambda_2 = -0.2057$.

The inherent multistability of this system is demonstated by the two sheets of dynamical regimes in the same area of the control parameters in fig. 3.

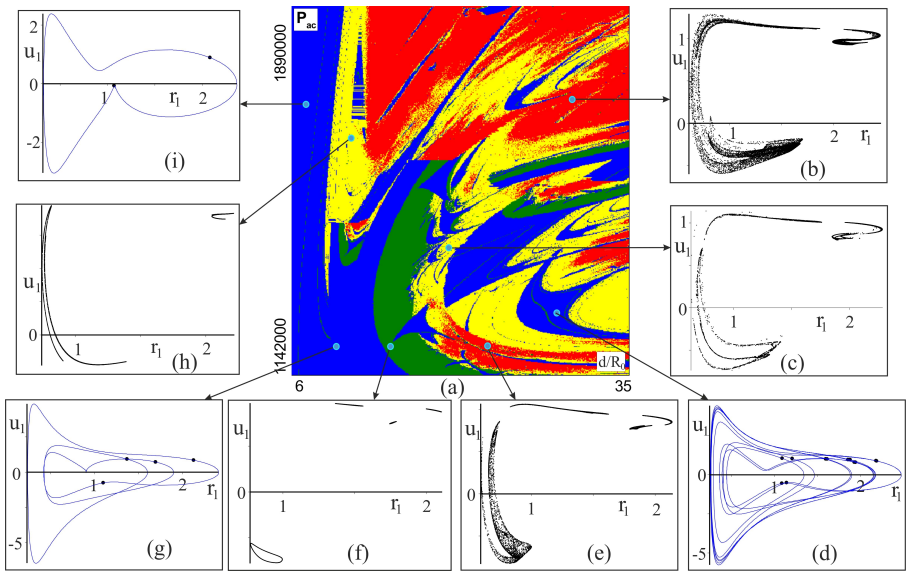

Figure 2: (a) Chart of the regimes of dynamics, (b)-(i) the projections of the phase portraits of the attractor, corresponding to some typical points of this chart. Black dots on the graphs correspond to the points on the Poincaré map and blue lines to the trajectories of the limit cycles. The following attractors are shown here: (b) hyperchaotic attractor at $d/R_0 = 32, P_{ac} = 1.68$ MPa; (c) synchronous chaotic attractor at $d/R_0 = 30, P_{ac} = 1.4$ MPa; (d) syncronous 12-periodic limit cycle at $d/R_0 = 28, P_{ac} = 1.3$ MPa; (e) hyperchaotic attractor at $d/R_0 = 22, P_{ac} = 1.2$ MPa; (f) quasiperiodic attractor at $d/R_0 = 14.5, P_{ac} = 1.2$ MPa; (g) asynchronous 4-periodic limit cycle at $d/R_0 = 10, P_{ac} = 1.2$ MPa; (h) synchronous chaotic attractor at $d/R_0 = 10, P_{ac} = 1.6$ MPa; (i) synchronous 2-periodic limit cycle at $d/R_0 = 6.75, P_{ac} = 1.7$ MPa.

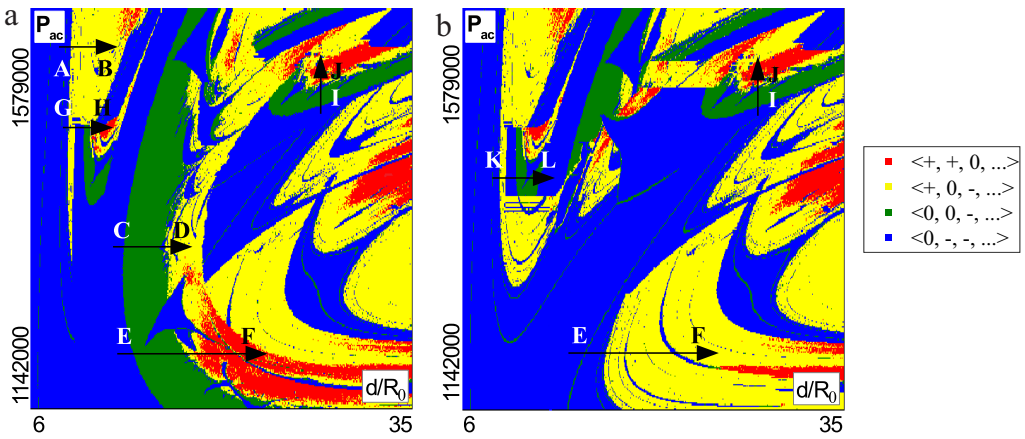

Figure 3: Two sheets of the charts of the regimes of dynamics in the following area: $P_{ac} \in [1.142, 1.579]$ MPa and $d/R_0 \in [6, 35]$, obtained for continuations of (a) an asynchronous limit cycle, (b) a synchronous limit cycle

We have shown in [1*] that synchronous chaotic attractors occur via the Feigenbaum cascade of period-doubling bifurcations, which begins from a stable synchronous limit cycle. For example, this scenario takes place in the parameter space along the path AB (see fig. 3).

We have established that asynchronous chaotic attractors appear according to the Afraimovich-Shilnikov scenario. It starts with a stable asynchronous limit cycle, and goes according to the following bifurcations sequence: the Neimark-Sacker bifurcation and emer-

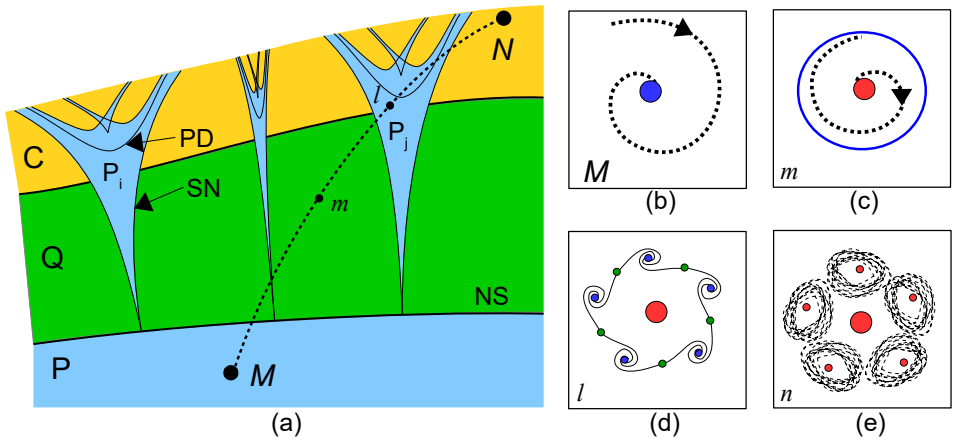

Figure 4: (a) Sketch of the bifurcation diagram illustrating bifurcations of a quasiperiodic regime. P, Q, Pi, and C – regions of the existence of (b) stable periodic orbit, (c) stable invariant torus, (d) resonant periodic orbits, and (e) chaotic attractors, respectively. MN – some path along which the chaotic attractor appears in accordance with the Afraimovich–Shilnikov scenario.

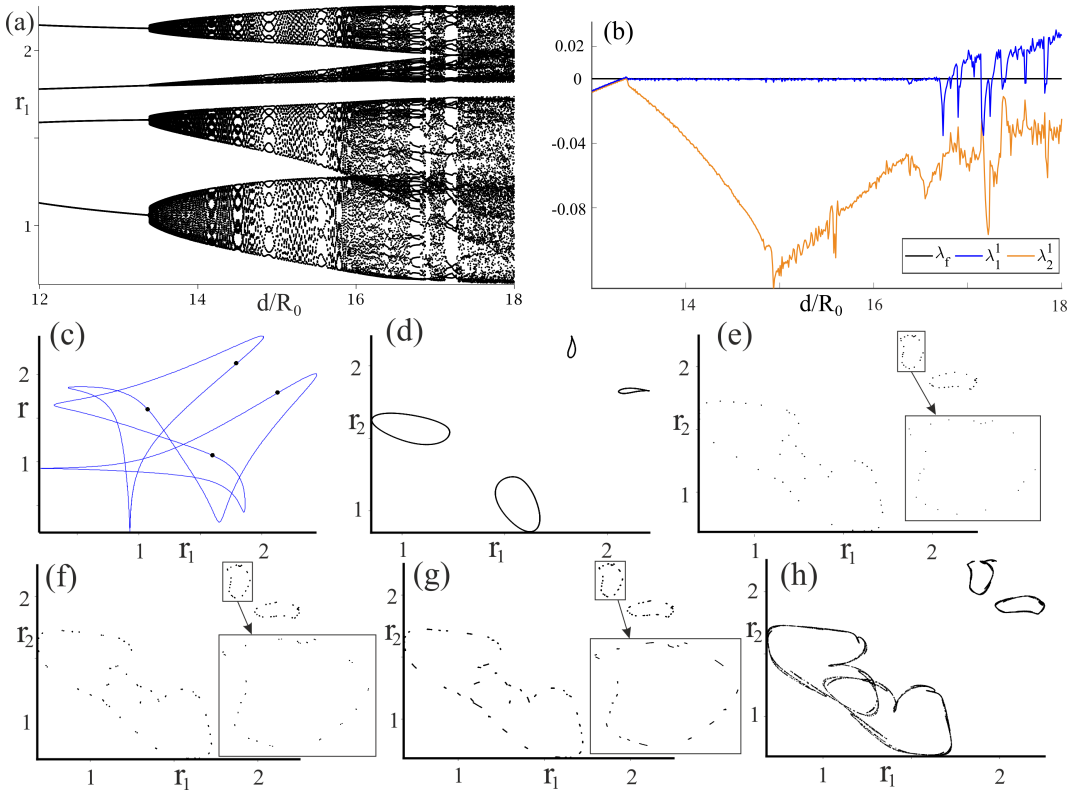

Figure 5: Implementation of the Afraimovich–Shilnikov scenario of onset of the chaotic attractor along path CD. (a) the bifurcation tree, (b) the graph of the largest Lyapunov exponents; (c)-(h) sequence of the projections of the Poincaré maps on the (r_1, r_2) plane, demonstrating the main stages of the scenario: (c) the stable periodic orbit of period 4, (d) the quasiperiodic regime, (e) resonant orbit, (f) the orbit of a doubled period, (g) strange chaotic attractor.

gence of a quasiperiodic regime; loss of stability of the quasiperiodic regime via a resonance and appearance of a stable asynchronous orbit; chaotic attractor appearing from the resonant

cycle, e.g. via the period-doubling cascade. The sketch of the bifurcation diagram, representing the Afraimovich-Shilnikov scenario is presented in fig. 4. An example of implementation of the Afraimovich-Shilnikov scenario with the graph of the largest Lyapunov exponents and a sequence of the phase portraits on the main stages of the scenario is presented in fig. 5. In fig. 5a we show the bifurcation tree, in fig. 5b the graph of the largest Lyapunov exponents is presented. The sequence of the Poincaré maps, illustrating the main stages of the scenario are shown in fig.-s 5c-h: fig. 5c shows stable periodic orbit of the period 4, fig. 5d demonstrates the invariant curve, corresponding to the quasiperiodic regime, fig. 5e corresponds to the resonant orbit, fig. 4f shows the stable orbit of doubled period, fig. 5g demonstrates the strange attractor after the Feigenbaum cascade, and fig. 5h represents the chaotic attractor with largest Lyapunov exponents $\lambda_1 = 0.0139, \lambda_2 = -0.0538$.

1.2.3 Scenario of emergence of hyperchaotic Shilnikov attractor

We have found two scenarios of onset of hyperchaotic attractors in the model of interacting microbubble contrast agents in the studied area of control parameters. The first one is related to the appearance of the homoclinic Shilnikov attractor.

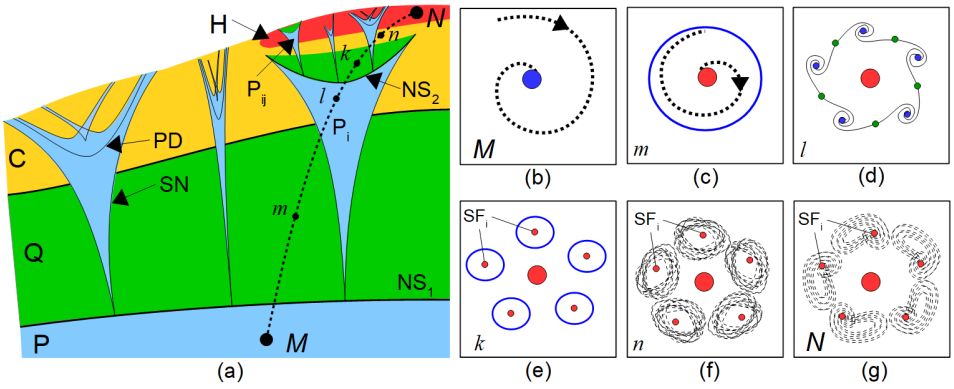

Figure 6: Sketch of the bifurcation diagram illustrating the scenario of onset of a hyperchaotic attractor in multidimensional maps ($N \geq 3$)

Assume there exists a stable asynchronous limit cycle. If it loses stability via the Neimark-Sacker bifurcation, simultaneously a quasiperiodic attractor appears. Later on, a resonance can occur, leading to appearance of the resonant orbit, which we denote as SF_i, while the quasiperiodic regimes becomes unstable. The next important step is the secondary Neimark-Sacker bifurcation of the periodic orbit. Because of it, SF_i becomes a saddle-focus with a two-dimensional unstable manifold. At the same time, a new quasiperiodic attractor appears.

The next step within the framework of this scenario is associated with the destruction of the stable quasiperiodic oscillations. It does not matter how it happens: through the Afraimovich–Shilnikov scenario, cascade of doubling bifurcations of the quasiperiodic regime or even via the tertiary Neimark–Sacker bifurcation. However, we suppose, and it is quite natural, that after the corresponding bifurcations, a chaotic attractor with one positive Lyapunov exponent appears (see fig. 6f).

The final and the key step in this scenario is the inclusion of the saddle-focus orbit SF_i into the chaotic attractor. After it, SF_i together with its two-dimensional unstable manifold and its

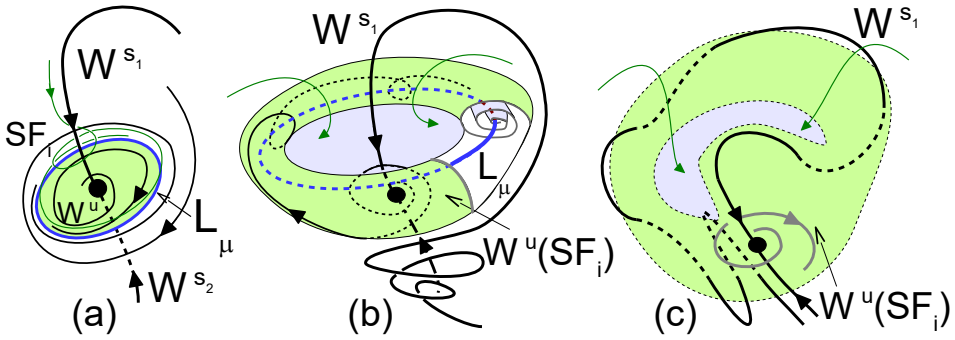

Figure 7: Possible scenario of the inclusion of saddle-focus periodic orbit SF_i into the chaotic attractor.

homoclinic structure belongs to the attractor, i.e. the discrete homoclinic Shilnikov attractor based on this saddle-focus orbit emerges (see fig. 6g). Orbits on this attractor can pass arbitrary close to SF_i, where two-dimensional areas are expanded. As a result, two Lyapunov exponents become positive.

Let us briefly clarify some details regarding the inclusion of SF_i into the attractor. Immediately after the Neimark–Sacker bifurcation, stable invariant curve L_μ is a node (see Fig. 7a). Then, this curve becomes of focal type, and the so-called Shilnikov funnel appears. After this, almost all orbits in the neighborhood of the saddle-focus are wound on the stable invariant curve (see fig. 7b). Furthermore, the size of the funnel is increased, and it approaches stable invariant manifold $W^{s_1}(SF_i)$. During this transition, orbits of the attractor approach closer and closer to the saddle-focus. Finally, the homoclinic intersection between stable and unstable manifolds of SF_i occurs, and the discrete Shilnikov attractor appears (see 7c). After this, the orbits on this attractor start pass arbitrarily close to the saddle-focus. The inclusion of a saddle-focus periodic orbit to the chaotic attractor can occur in different ways. It depends on the transition from the secondary quasiperiodic regime to the chaotic attractor. In the model of microbubble contrast agents, as well as in other well-known examples exhibiting the appearance of the discrete Shilnikov attractor, the inclusion happens in a soft manner by a smooth transformation of the chaotic attractor (see [65–67]).

The implementation of the proposed scenario of appearance of a hyperchaotic attractor in the model of two coupled microbubble contrast agents was shown numerically in work [1*]. The implementation of this scenario along the path EF in the parameter space ($P_{ac} = 1.2$ MPa, $13 < d/R_0 < 25$) is illustrated in fig. 8. The bifurcation tree, corresponding to this route is shown in fig. 8a and the graph of two largest Lyapunov exponents is presented in fig. 8b. Projections of the Poincaré sections for some attractors along the route are shown in fig.-s 8c-h. fig. 8c corresponds to the quasiperiodic oscillations, emerging with the first Neimark–Sacker bifurcation. With increasing d a resonance occurs (see fig. 8d). Then it undergoes the secondary Neimark–Sacker bifurcation, becoming a saddle-focus with two-dimensional unstable manifold, while at the same time a new quasiperiodic regime appears (see fig. 8e). After that, a stable high-periodic resonant orbit appears (see fig. 8f). It goes through the cascade of period-doubling bifurcations, which leads to the onset of the chaotic attractor (see fig. 8g). Finally, the inclusion of the saddle-focus orbit into the chaotic attractor leads to emergence

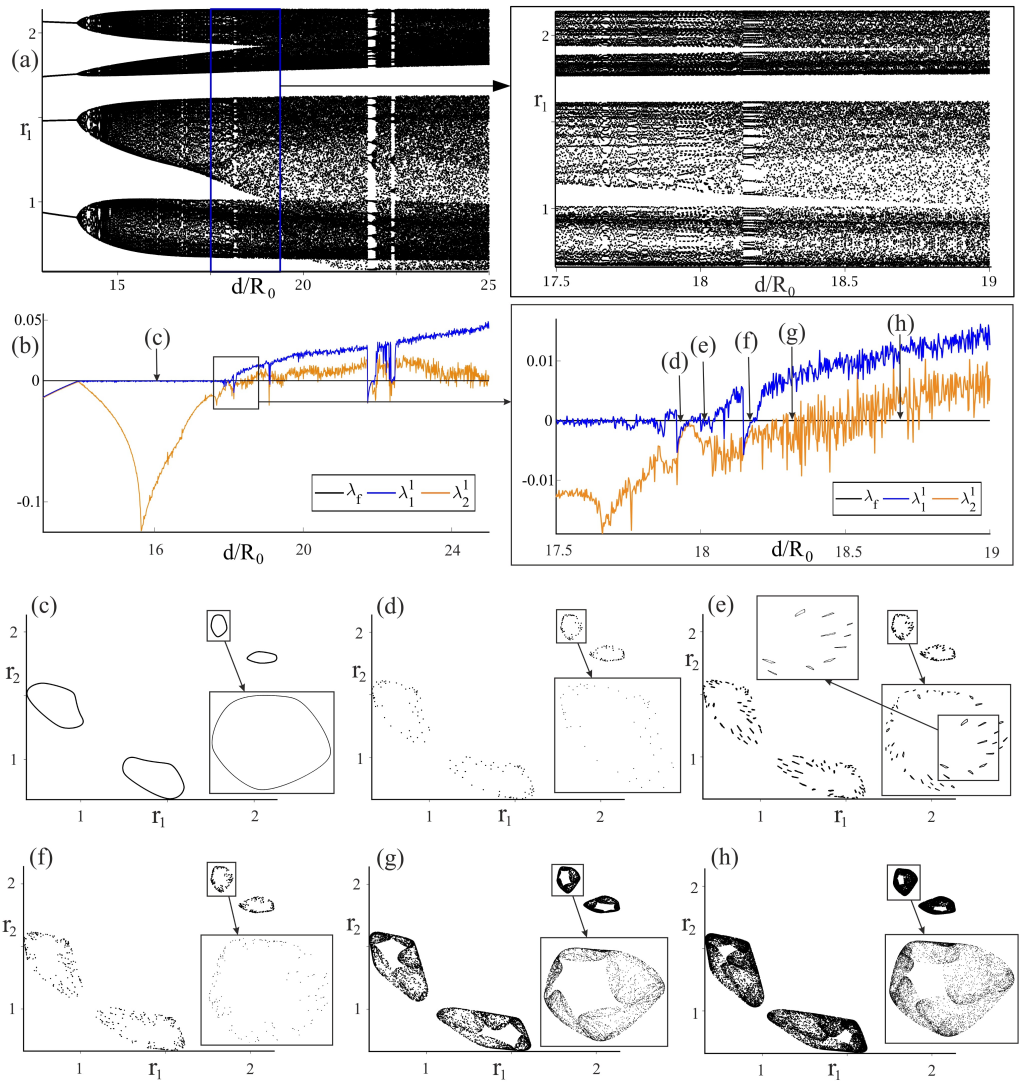

Figure 8: Implementation of the scenario of transition to hyperchaos with emergence of the discrete Shilnikov attractor on the path EF: (a) the bifurcation tree, (b) the graph of the largest Lyapunov exponents, and the projections of the Poincaré maps on (r_1, r_2) subspace, demonstrating the main steps of the scenario: (c) quasiperiodic regime, (d) resonant orbit, (e) secondary quasiperiodic regime, (f) resonant limit cycle after destruction of the secondary quasiperiodic regime, (g) chaotic attractor, (h) hyperchaotic attractor.

of the hyperchaotic dynamics (see fig. 8h). The largest Lyapunov exponents corresponding to such attractor at $d = 18.71$ have the following values: $\lambda_1 = 0.0135, \lambda_2 = 0.0019, \lambda_3 = -0.5560$.

1.2.4 Scenario of appearance of a hyperchaotic attractor based on the destruction of synchronization

The second scenario of appearance of hyperchaotic attractors in the model of interacting contrast agents is related to the loss of transversal stability by a synchronous chaotic attractor.

Assume there exists a synchronous stable limit cycle. Suppose the Feigenbaum cascade happens, and each subsequent limit cycle remains within the synchronization manifold Fix(S), maintaining transversal stability. Thus, a synchronous chaotic attractor appears. Occurrence of such regimes according to this scenario in the model of coupled contrast agents was demon-

strated in [1*], [3*]. Such synchronous attractor contains a countable set of transversally stable saddle orbits. Their unstable manifolds belong to Fix(S). Since each orbit on the attractor is transversally stable, we observe strong synchronization at this step.

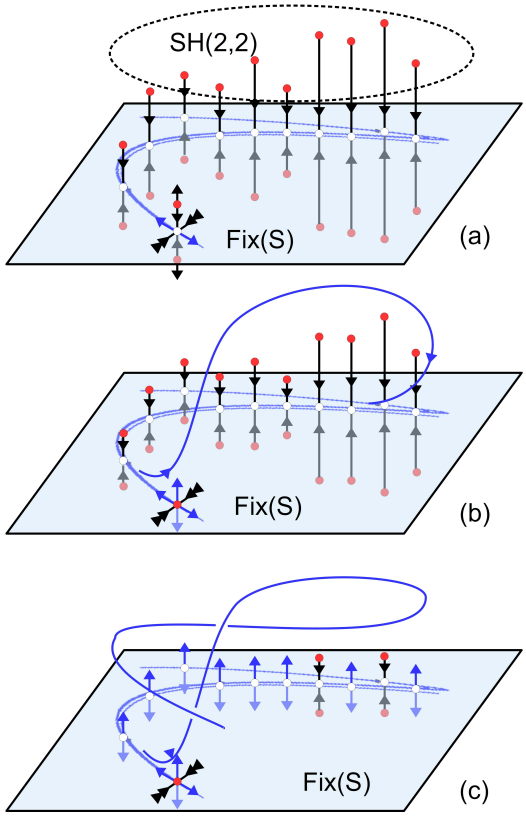

Figure 9: Scheme of the main steps of the bubbling transition scenario.

If pairs of saddle orbits with two directions of instability exist outside of Fix(S), they can form heteroclinic manifolds with transversally stable saddle trajectories belonging to the synchronous attractor. If we further increase the bifurcation parameter, these triplets of two asynchronous orbits and a synchronous one can merge via the subcritical pitchfork bifurcation. Thus, orbits with with two-dimensional unstable manifolds appear in the synchronous attractor. Notice that one of the directions of instability is transversal to Fix(S) (see fig. 9). A cascade of such bifurcations leads to appearance of a transversally unstable set of a positive measure inside the synchronization manifold. A trajectory in Fix(s) passing through a neighborhood of such set can be ejected outside of the synchronization manifold. Subsequently, the trajectory can return into Fix(S) through a transversally stable domain. At this step, the synchronous invariant set becomes a Milnor attractor with a riddled basin [33], which is transversally stable on average. Thus, the orbit can be naturally split into two components: synchronous (inside Fix(S)) and asynchronous (outside of Fix(S)). In the beginning of the bifurcation cascade, the fraction of time corresponding to the asynchronous component is very small, and the ejection of the orbit outside of Fix(S) happens so rarely it can be considered an extreme event [63]. Because the trajectory outside of Fix(S) passes close to the saddle orbits with two-dimensional unstable manifolds, the dynamics within the asynchronous component is always hyperchaotic. While the synchronization manifold is transversally stable on average, the trajectory keeps returning back

into Fix(S) through the transversally stable domains, and we observe weak synchronization. If the cascade of the subcritical pitchfork bifurcations continues, the synchronous invariant set in Fix(S) becomes transversally unstable on average. Thus the influence of the asynchronous component on the dynamics grows, and the regime becomes hyperchaotic.

We have demonstrated the implementation of the aforementioned scenario of emergence of hyperchaotic oscillations in the model of coupled contrast agents in [3*] (see fig. 10). We present the graph of largest Lyapunov exponents in fig. 10a, the graph of the Lyapunov exponents associated with synchronous and asynchronous components in fig. 10b, the graph of the fractions of time attributed to the synchronous and asynchronous components of a typical orbit on the attractor in fig. 10c and the graph of the largest transversal Lyapunov exponent in fig. 10d.

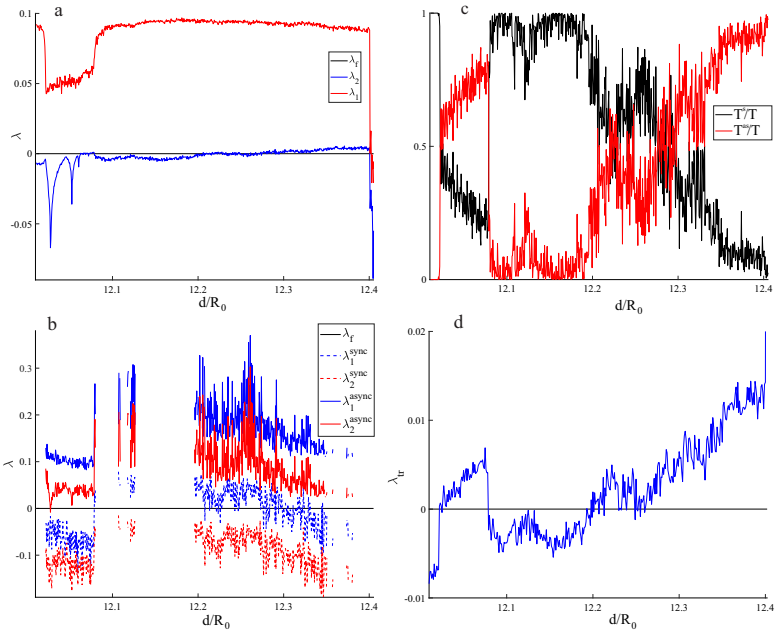

Figure 10: (a) The graph of the largest Lyapunov exponents for attractor as a whole , (b) the graph of the largest Lyapunov exponents for the synchronous and the asynchronous components, (c) the graph of the fractions of the synchronous and the asynchronous components, (d) the largest transversal Lyapunov exponent.

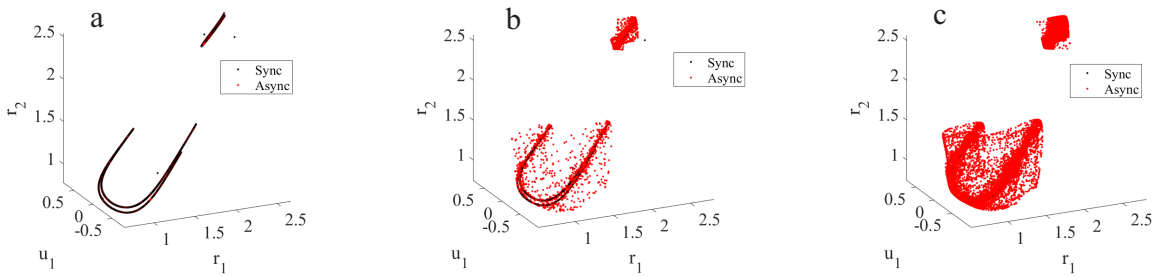

Figure 11: The sequence of the projections of the Poincaré maps on (r_1, u_1, r_2) for (a) $d = 12.18$, (b) $d = 12.27$, (c) $d = 12.36$.

We show the sequence of the projections of the Poincaré maps on the subspace (r_1, u_1, r_2), demonstrating the growth of the fraction of points in the Poincaré map, corresponding to

the asynchronous component and the gradual loss of transversal stability in fig. 11. The chaotic attractor existing at $d/R_{10} = 12.18$ is shown in fig. 11a. It is characterized by the largest Lyapunov exponents $\lambda_1 = 0.0953$, $\lambda_2 = -0.0032$, the largest transversal Lyapunov exponent $\lambda_{tr} = -0.0027$ and the fraction of time, associated with the asynchronous component, $T^{as}/T = 0.037$. For the regime at $d/R_{10} = 12.27$ this ratio is $T^{as}/T = 0.338$ (see fig. 11b). The largest Lyapunov exponents at this point have values $\lambda_1 = 0.0940$, $\lambda_2 = -0.0006$, and the corresponding values for the synchronous and the asycnhronous components are $\lambda_1^s = 0.0528, \lambda_2^s = -0.0410$ and $\lambda_1^{as} = 0.1747$, $\lambda_2^{as} = 0.0786$. One can see that the dynamics inside Fix(S) is chaotic, while it is hyperchaotic outside of it, which proves that there are two-dimensional instabilities in the asynchronous saddle set. At this point the largest transversal Lyapunov exponent has small positive value $\lambda_{tr} = 0.0010$. At $d/R_{10} = 12.36$ the synchronous invariant set is transversally unstable with the largest transversal Lyapunov exponent $\lambda_{tr} = 0.0112$. The ratio of time attributed to the asynchronous becomes $T^{as}/T = 0.636$. This fact together with the two-dimensional instabilities outside of Fix(S), characterized by $\lambda_1^{as} = 0.1124, \lambda_2^{as} = 0.0242$, leads to hyperchaotic dynamics with the following largest Lyapunov exponents $\lambda_1 = 0.0908$, $\lambda_2 = 0.0037$.

1.2.5 Stability with respect to symmetry breaking

In case of fully identical bubbles, system (7) is symmetrical with respect to the change of variables $R_1 \leftrightarrow R_2, \dot{R}_1 \leftrightarrow \dot{R}_2$. However, perturbation in the equilibrium radius of on of the bubbles R_{i0} break this symmetry. In work [2*] we considered stability of the main dynamical regimes with respect to the following perturbations breaking the symmetry:

$$R_{20} = \varepsilon R_{10}, \quad (|\varepsilon - 1| \ll 1). \tag{8}$$

We show that multistability is the main factor affecting the stability of synchronous regimes to a perturbation of the equilibrium radius of one of the bubbles. If the system is monostable, then the synchronous attractor is stable to such perturbations in the following sense: the attractor gradually transforms with changes of the control parameter. In case of multistability, if the synchronous attractor coexists with an asynchronous limit cycle or a quasiperiodc regime, it will also likely be stable with respect to the symmetry breaking perturbations, but in a more narrow range of ε then in the monostable case.

If a synchronous attractor coexists with an asynchronous chaotic one, there are different possibilities depending on the particular values of parameters: it can be either stable to the symmetry breaking in a range of ε similar to the case of coexistence with an asynchronous limit cycle, or unstable to even very small perturbations of ε. If a synchronous attractor coexists with a hyperchaotic one, it is always unstable to the symmetry breaking perturbations.

The impact of multistability on the stability of synchronous regimes can be illustrated by the following example. The system is monostable at $P_{ac} = 1.8$ MPa, $d/R_{10} = 11.3$. Namely, only the synchronous chaotic attractor shown in fig. 12a exists. In this case, qualitative properties of this dynamical regime persist in quite a wide range of ε (see fig. 12b). Note that a new chaotic attractor emerges at high values of ε. Its consideration goes beyond the study of stability of the synchronous regimes (see [2*] for details). Continuation of the synchronous chaotic regime at $P_{ac} = 1.8$ MPa, $d/R_{10} = 11.47$ is also a synchronous chaotic one. However,

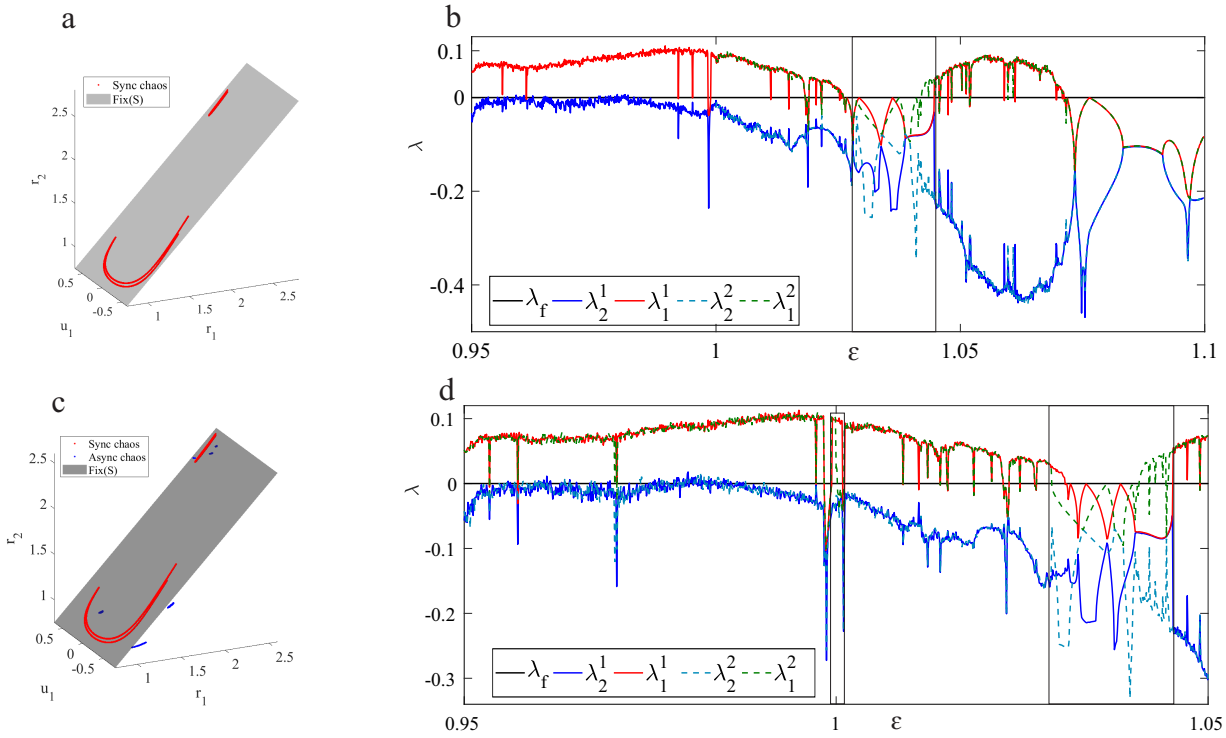

Figure 12: Projections of the Poincaré maps of (a) synchronous chaotic attractor at $P_{ac} = 1.8 \cdot 10^6, d/R_{10} = 11.3$, (c) coexisting synchronous and asynchronous chaotic attractors at $P_{ac} = 1.8 \cdot 10^6, d/R_{10} = 11.47$. (b), (d) graphs of the largest Lyapunov exponents of the continuations of the corresponding attractors.

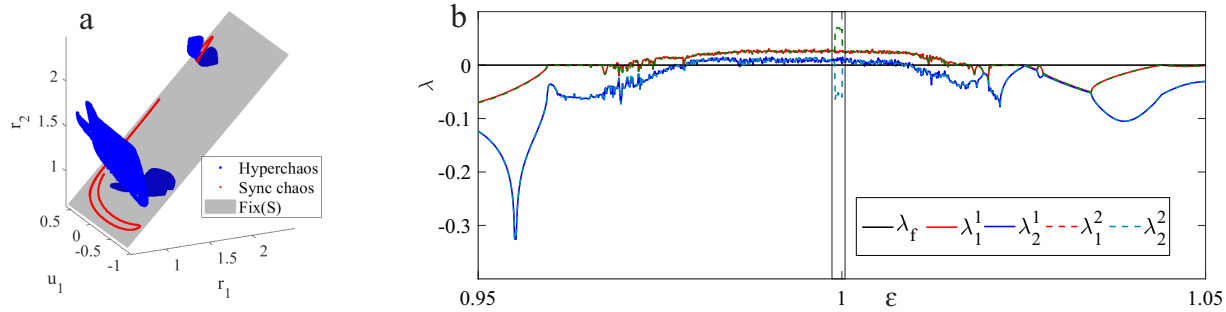

Figure 13: (a) Projections of the Poincaré maps of the synchronous chaotic attractor and the hyperchaotic one at $P_{ac} = 1.2$ MPa, $d/R_{10} = 21$ on the (r_1, u_1, r_2) subspace, (b) graph of the largest Lyapunov exponents of their continuation by the ε parameter.

at this values of the control parameters an asynchronous chaotic attractor coexists with it. In this case, the synchronous regime is unstable with respect to the perturbations of ε, while the asynchronous one persists in a wide range of the parameter.

On the other hand, hyperchaotic attractors are stable with respect to symmetry breaking. An example of a hyperchaotic regime coexisting with a synchronous chaotic one is presented in fig. 13. Here the hyperchaotic attractor is stable to the symmetry breaking perturbations in a wide range of ε, while the synchronous chaotic one is not.

We have also shown that attractors appearing on the main steps of the scenario of emergence of hyperchaotic dynamics based on the destruction of synchronization via the bubbling transition are also stable to the symmetry breaking perturbation.

1.3 The model of interacting neurons

1.3.1 The model of two interacting neurons

Consider a resting neuron. From the dynamical systems perspective this state is described by a stable equilibrium. The inputs coming through the synapses can change the membrane potential and produce postsynaptic potentials. Voltage-sensitive ion channels embedded in the membrane can amplify certain postsynaptic potentials leading to an abrupt increase in the membrane voltage that propagates to other neurons via an axon – a *spike*, or *action potential*. [68]. Bursting refers to the state of a neuron, in which it fires discrete groups of spikes (bursts), separated by period of quiescence [69; 70].

Here we use the Hindmarsh-Rose system to model neuronal activity [22]. It reproduces both spiking and bursting firing patterns fairly well. The model of two neurons coupled via a direct electrical connection between the membranes is governed by the following system of equations:

$$\begin{aligned}
\dot{x}_1 &= y_1 - ax_1^3 + bx_1^2 - z_1 + I + D_0(x_2 - x_1),\\
\dot{y}_1 &= c - dx_1^2 - y_1,\\
\dot{z}_1 &= r(s(x_1 - x^0) - z_1),\\
\dot{x}_2 &= y_2 - ax_2^3 + bx_2^2 - z_2 + I + D_0(x_1 - x_2),\\
\dot{y}_2 &= c - dx_2^2 - y_2,\\
\dot{z}_2 &= r(s(x_2 - x^0) - z_2),
\end{aligned} \tag{9}$$

where x_i refers to the membrane potential of i-th neuron, y_i and z_i correspond to the fast and slow ionic currents respectively, $i = 1, 2$. We consider two identical neurons, thus choosing the same parameters for both of them $a = 1$, $b = 3$, $c = 1$, $d = 5$, $s = 4$, $x^0 = -8/5$ [45; 46]. System (9) is a slow-fast one, because of the small parameter $r = 0.0021$. The constant current I, applied to both neurons, is treated as the control parameter.

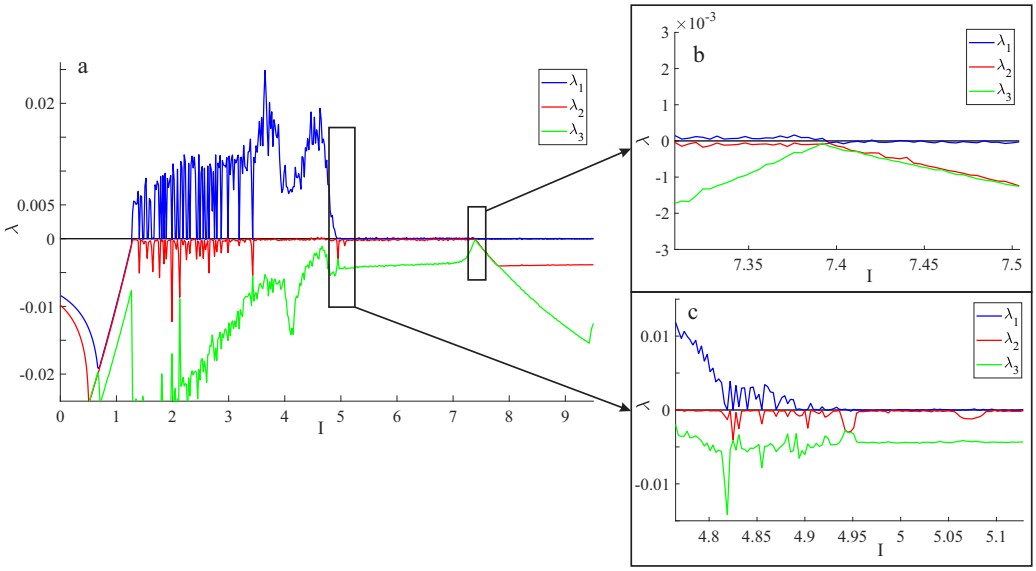

Figure 14: The largest Lyapunov exponents corresponding to system (9) in the range $0 < I < 9.5$.

In [4*] we studied the intervals of transversal stability of the synchronous invariant sets, corresponding to the attractors found earlier in the single neuron model in [42]. We establish

that the asynchronous chaotic attractor emerges according to the Afraimovich-Shilnikov scenario. We also show that the asynchronous chaotic regime is stable in a wide range of control parameters. The graph of the largest Lyapunov exponents by parameter I is presented in fig. 14. Besides that, we demonstrate that among all the synchronous regimes, only the stable equilibria and spiking limit cycles are stable, while the bursting regimes (chaotic, as well as periodic) are transversally unstable in the entire domain of their existence.

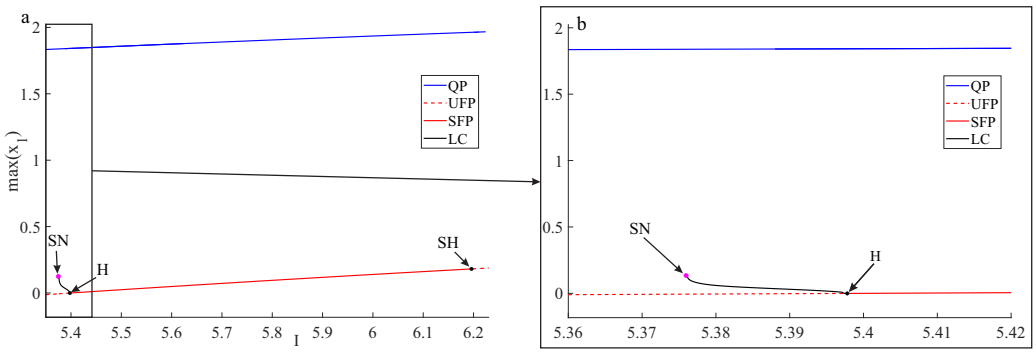

Figure 15: Bifurcation diagram in the first domain of bistability $5.35 < I < 6.25$. Here SH denotes subcritical Andronov-Hopf bifurcation, H - supercritical Andronov-Hopf bifurcation, SN – saddle-node bifurcation of the limit cycle.

In the studied range of I, there are two domains of bistability, in which synchronous and asynchronous regimes coexist. In the first one the equilibrium becomes stable via the subcritical Andronov-Hopf bifurcation with decreasing I, and it coexists with asynchronous quasiperiodic oscillations in the interval $5.398 < I < 6.198$ (see fig. 15). The synchronous fixed point then loses stability via the supercritical Andronov-Hopf bifurcation at $I = 5.398$, thus giving rise to a stable limit cycle, existing in a narrow range of the control parameter. It coexists with the quasiperiodic attractor before disappearing via the limit cycle saddle-node bifurcation (see fig. 15).

Right after its appearance, the chaotic attractor corresponds to asynchronous tonic spiking of both neurons. With decreasing I a soft transition to chaotic asynchronous bursting occurs. At $I = 4.3080$ one can see chaotic spiking with occasional anomalous interval of quiescence (see fig. 16a). As I decreases, such resting periods expand and become more frequent (see fig. 16b). Gradually, one can start to distinguish distinct bursts separated by the resting periods (see fig. 16c). At low values of the current, bursts consisting of 2-3 spikes can be observed (see fig. 16d). Note that the value of current, corresponding to fig. 16c fall into windows of stability of the asynchronous chaotic attractor, thus regular bursting is depicted.

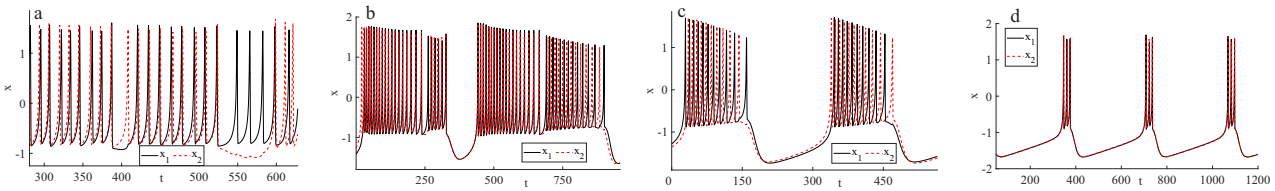

Figure 16: (a) Chaotic spiking at $I = 4.3080$, (b) chaotic regime in-between spiking and bursting at $I = 3.7880$, (c) regular bursting at $I = 2.428$, (d) regular bursting at $I = 2.960$.

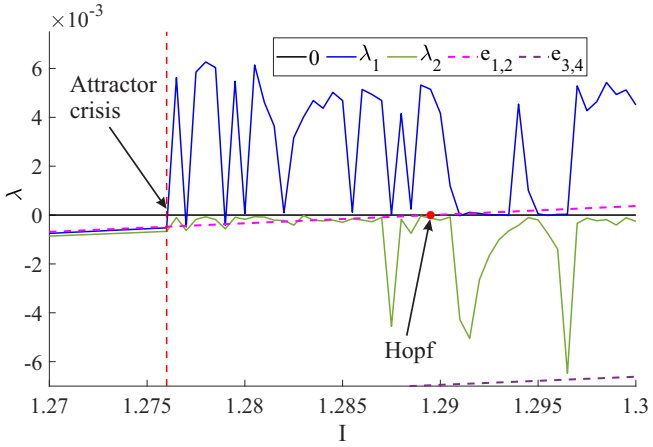

Figure 17: Bifurcation diagram in the second domain of bistability of system (9), $1.27 < I < 1.30$.

The second domain of bistability exists in the following range: $1.2760 < I < 1.2895$. The synchronous equilibrium becomes stable via the subcritical Andronov-Hopf bifurcation. It coexists with the asynchronous chaotic attractor, corresponding to tonic bursting of the neurons (see fig. 17). We describe the likely mechanism of the crisis of the asynchronous attractor with decreasing I in [5*]. We also studied changes of the stable equilibrium type depending on the parameter. We have shown that in the domain of bistability the equilibrium is a focus, and the system close to the subcritical Andronov-Hopf bifurcation is excitable, having properties of the resonators according to the classification given in [68].

1.3.2 Excitation of the system of two neurons by a signal from an external neuron

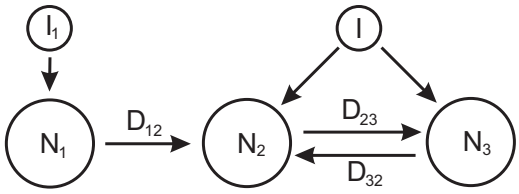

Figure 18: Scheme of excitation of the system of two neurons by the third one via a directional connection.

Let us consider the following system of three neurons with directional couplings: the first neuron has only a one-directional connection to the second neuron, and the second and the third neurons form a fully-connected group (see fig. 18). If the Hindmarsh-Rose system is used as the model of behavior for each of the neurons, and the electrical couplings are represented linearly in equations, the governing system of equations looks as follows:

$$
\begin{aligned}
\dot{x}_1 &= y_1 - ax_1^3 + bx_1^2 - z_1 + I_1, \\
\dot{y}_1 &= c - dx_1^2 - y_1, \\
\dot{z}_1 &= r(s(x_1 - x^0) - z_1), \\
\dot{x}_2 &= y_2 - ax_2^3 + bx_2^2 - z_2 + I_2 + +D_{32}(x_3 - x_2) + D_{12}(x_1 - x_2), \\
\dot{y}_2 &= c - dx_2^2 - y_2, \\
\dot{z}_2 &= r(s(x_2 - x^0) - z_2), \\
\dot{x}_3 &= y_3 - ax_3^3 + bx_3^2 - z_3 + I_3 + D_{23}(x_2 - x_3), \\
\dot{y}_3 &= c - dx_3^2 - y_3, \\
\dot{z}_3 &= r(s(x_3 - x^0) - z_3),
\end{aligned}
\tag{10}
$$

where the same notation as in system (9) is used. In this configuration the first neuron plays the role of a signal generator, while the system of the form (9) is considered the slave system receiving the excitatory signal. It allows us to study the influence of signals, occurring naturally in biological neuronal networks, on such group of two neuron.

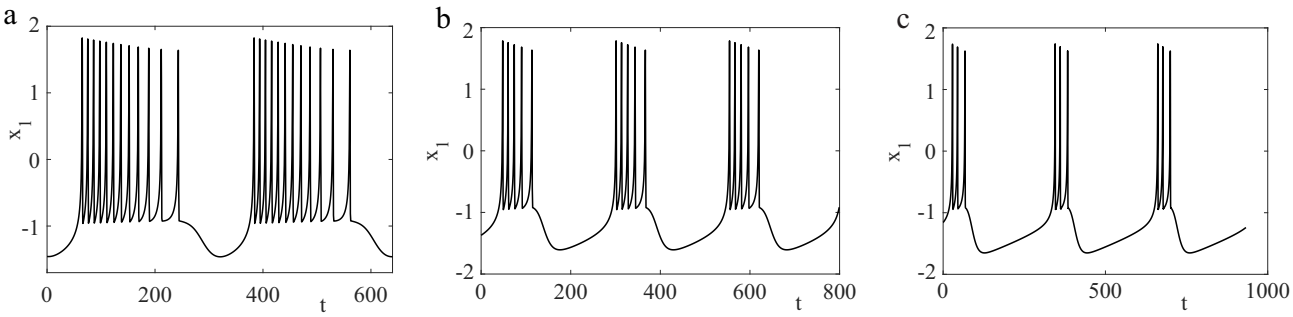

Figure 19: Signals, generated by the first neuron at (a) $I_1 = 3.20$, (b) $I_1 = 2.00$, (c) $I_1 = 1.40$.

We perform spectral analysis of the signals generated by the first neuron applying the fast Fourier transform (FFT) to the numerical solutions to estimate their periods and mean intraburst interspike intervals. We calculate the eigenvalues of the Jacobi matrix in the fixed point to find the periods of small damped oscillations in the neighborhood of the stable equilibrium. We have shown that bursting signals with long periods are suitable for excitation of the slave system in the domain of small external currents, while spiking signals are ineffective in this case. We considered three regular bursting regimes as excitatory signals: the one with 12 spikes per burst with period $T_0^b = 318.48$ generated by the master neuron at $I_1 = 3.2$; bursting with 5 spikes per burst with inter-burst interval $T_1^b = 252.53$ created by the master neuron at $I_1 = 3.2$; bursting with 3 spikes per burst with inter-burst interval $T_2^b = 316.46$, generated by the first neuron at $I_1 = 1.4$ (see fig. 19). We also considered regular spiking excitatory signal with inter-spike interval $T_1^s = 8.10$ generated by the external neuron at $I_1 = 3.5$.

The chart of excitation of the slave system by the bursting signal generated by the master neuron at $I_1 = 3.20$, and the chart regular and chaotic dynamics under such excitation are presented in fig. 20. In fig. 20 zone (I) corresponds to tonic bursting of both neurons of the slave system, while zone (II) – to subthreshold oscillations of both neurons (after the transient process), and zone (III) – to tonic bursting of the second neuron, while the third one exhibits subthreshold oscillations. Examples of the resulting regimes of oscillations from all three zones are presented in fig. 21.

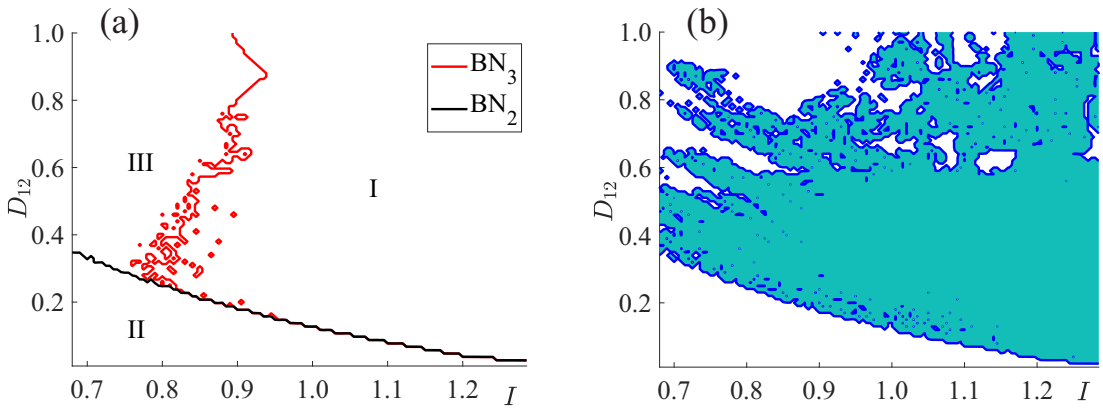

Figure 20: (a) Boundaries of excitation of the slave system by the signal from master neuron in the following domain of control parameters: $0.680 < I < 1.285, 0 < D_{12} < 1$, (b) the domains of chaotic (filled) and regular (non-filled) dynamics

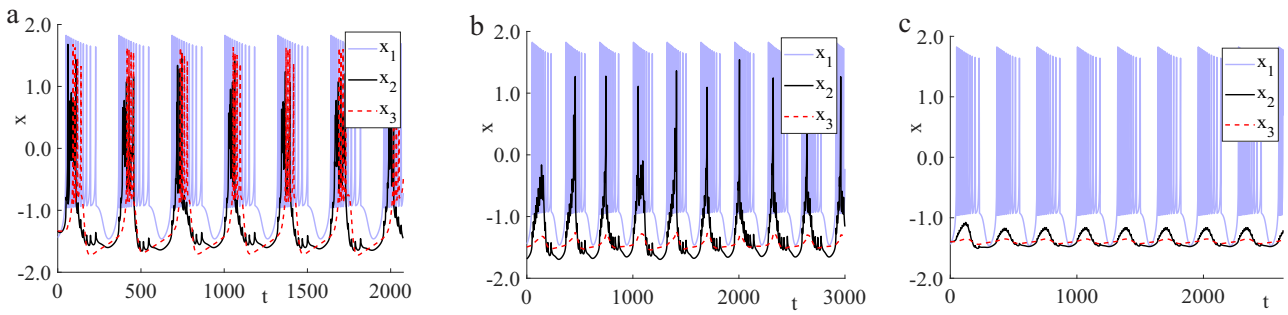

Figure 21: Different firing patterns of the slave system excited by regular signal, generated by the external neuron at $I_1 = 3.20$. (a) Chaotic bursting at $I = 1.25, D_{12} = 0.5$ (zone I), (b) chaotic bursting of the second neuron and subthreshold oscillations of the third one at $D_{12} = 0.6, I = 0.75$ (zone III), (c) regular subthreshold oscillations of both neurons of the slave system at $I = 1.0, D_{12} = 0.10$ (zone II).

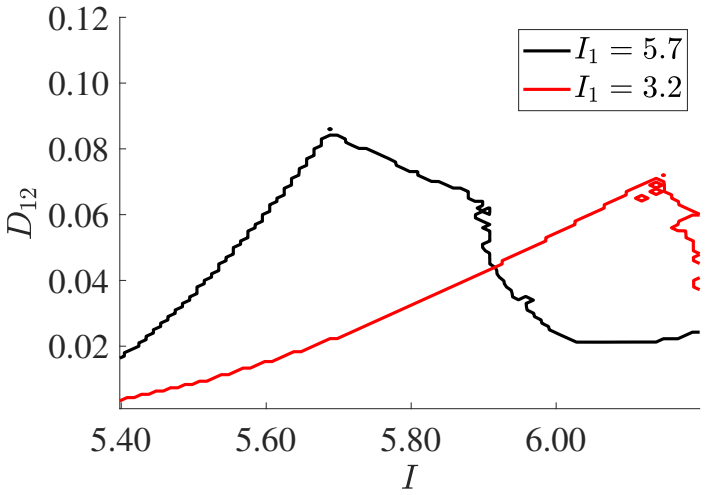

Figure 22: Boundaries of excitation of the slave system in the domain of bistbility $5.398 < I < 6.198, 0 < D_{12} < 0.12$ by (a) bursting signal, generated by the master neuron at $I_1 = 3.2$, (b) spiking signal, generated by the master neuron at $I_1 = 5.7$.

We also studied exctiation of the slave system by various signals in another domain of bistability of the system of two neurons: $5.398 < I < 6.198$. The boundaries of excitation by different signals are presented in fig. 22. In this interval of currents, upon successful excitation of the slave system, the resulting firing pattern is tonic spiking, regardless of whether the incoming signal is a bursting or spiking one. The regime after the transient process is close to the quasiperiodic spiking oscillations, existing in the system of two neurons at the corresponding value of I in the absence of the external influence. For example, excitation the slave system at $I = 5.5, D_{12} = 0.03$ by the bursting signal, generated by the first neuron at $I_1 = 3.20$, leads to the mean interspike interval T close to the corresponding interval T_q of the quasiperiodic oscillations at $I = 5.5$ in the group of two neurons: $T/T_q = 0.9903$. The main factor, responsible for the excitability of the system in this area of the control parameters is bistbility. The external signal can force the slave system to transition over the separatrix to the basin of the quasiperiodic attractor. However, its influence becomes relatively small after the transient process, and can be considered a small perturbation to the quasiperiodic oscillations of the slave system.

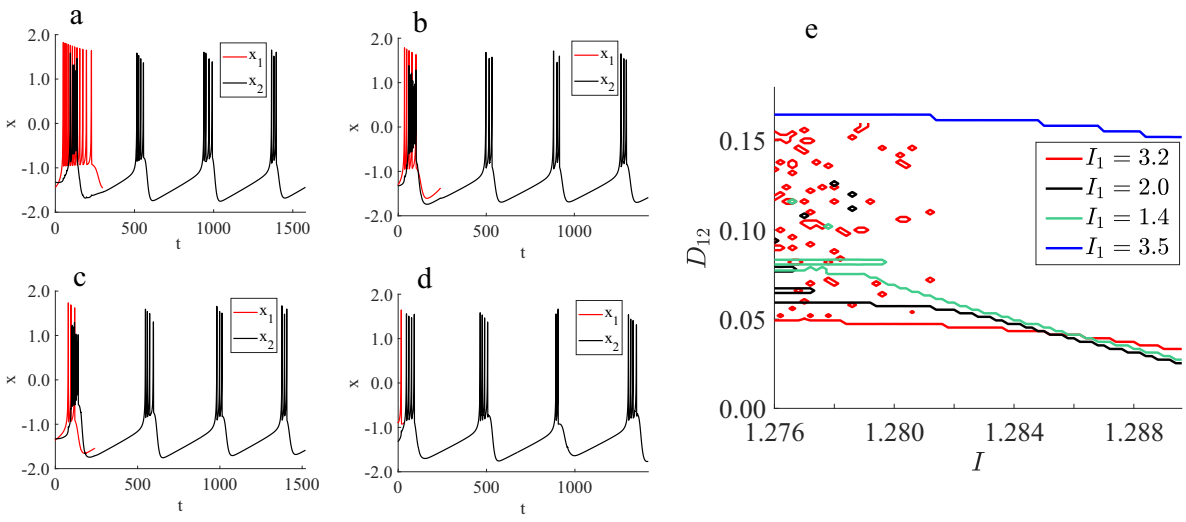

Figure 23: Examples of excitation of the slave system at $I = 1.284$ by a single period of several different excitatory signals from the master neuron at the following values of parameters of the current I_1 and the coupling strength D_{12}: (a) $D_{12} = 0.1, I_1 = 3.2$, (b) $D_{12} = 0.1, I_1 = 2.0$, (c) $D_{12} = 0.1, I_1 = 1.4$, (d) $D_{12} = 0.2, I_1 = 3.5$. (e) the borderlines of excitation of the slave system in the bistability domain $1.2760 < I < 1.2895, 0 < D_{12} < 0.18$ by the excitatory signals generated by the first neuron at the following currents: red – $I_1 = 3.20$, black – $I_1 = 2.00$, green – $I_1 = 1.4$, blue – $I_1 = 3.5$.

Besides that, we studied the possibility of excitation of the slave system by a single period of a regular excitatory signal in the domain of bistability $1.2760 < I < 1.2895$. We demonstrate examples of excitation of the system of two neuron by different finite signals in fig.-s 23a-d. We present the chart showing boundaries of the domains of excitation of the slave system for four different signals in fig. 23e.

2 Conclusion

In this work we have studied two systems of coupled nonlinear oscillators occurring in biophysical applications: the model of interacting microbubble contrast agents and the model of coupled neurons. We have obtained the following results:

1. We have proposed a mathematical model, describing dynamics of two contrast agents encapsulated in shells interacting via the Bjerknes force.

2. We have developed a software package for numerical studying of dynamics in the considered models. It allows us to compute individual orbits, construct the Poincaré maps, to find Fourier transforms of the solutions, to calculate the spectrum of the Lyapunov exponents, including separate computing of the spectrum for the synchronous and the asynchronous components of a trajectory, to calculate the largest transversal Lyapunov exponent, to construct one- and two-dimensional charts of the dynamical regimes while using the numerical continuation method for obtaining the initial conditions.

3. We have found the domains in the parameter space, where the synchronization of the contrast agents oscillations takes place. We studied the scenarios of emergence of synchronous and asynchronous dynamical regimes and the phenomenon of destruction of synchronization.

4. We studied dynamics in the system of two electrically coupled neurons, described by the Hindmarsh-Rose system. We have found domains of stability of the synchronous regimes of dynamics and explained the scenario of occurrence of the asynchronous chaotic attractor.

5. We have explained the underlying mechanisms responsible for excitability of the fully-connected group of two neurons in the domains of stability of the synchronous equilibrium. We have performed modeling of excitation of this system by an external signal, generated by a separate neuron.

References

1. *Strogatz S. H.* Nonlinear dynamics and chaos: with applications to physics, biology, chemistry, and engineering. — CRC press, 2018.
2. *Pikovsky A.*, *Politi A.* Lyapunov Exponents: A Tool to Explore Complex Dynamics. — Cambridge University Press, 2016.
3. *Skokos C.* — Berlin, Heidelberg : Springer Berlin Heidelberg, 2010. — P. 63–135.
4. *Vulpiani A.*, *Cecconi F.*, *Cencini M.* Chaos: from simple models to complex systems. Vol. 17. — World Scientific, 2009.
5. *Klibanov A. L.* Microbubble contrast agents: targeted ultrasound imaging and ultrasound-assisted drug-delivery applications // Investigative radiology. — 2006. — Vol. 41, no. 3. — P. 354–362.
6. *Hoff L.* Acoustic characterization of contrast agents for medical ultrasound imaging. — Springer Science & Business Media, 2001.
7. *Goldberg B.*, *Raichlen J.*, *Forsberg F.* Ultrasound Contrast Agents: Basic Principles and Clinical Applications. — Taylor & Francis, 2001.
8. *Szabo T. L.* Diagnostic ultrasound imaging: inside out. — Academic press, 2004.
9. *Doinikov A. A.*, *Bouakaz A.* Review of shell models for contrast agent microbubbles // IEEE transactions on ultrasonics, ferroelectrics, and frequency control. — 2011. — Vol. 58, no. 5. — P. 981–993.
10. Material characterization of the encapsulation of an ultrasound contrast microbubble and its subharmonic response: Strain-softening interfacial elasticity model / S. Paul, A. Katiyar, K. Sarkar, D. Chatterjee, W. T. Shi, F. Forsberg // The Journal of the Acoustical Society of America. — 2010. — Vol. 127, no. 6. — P. 3846–3857.
11. *Plesset M. S.* The dynamics of cavitation bubbles // Journal of Applied Mechanics. — 1949. — Vol. 16, no. 3. — P. 277–282.
12. Absorption and scatter of encapsulated gas filled microspheres: theoretical considerations and some measurements / N. de Jong, L. Hoff, T. Skotland, N. Bom // Ultrasonics. — 1992. — Vol. 30, no. 2. — P. 95–103.
13. A model for large amplitude oscillations of coated bubbles accounting for buckling and rupture / P. Marmottant, S. Van Der Meer, M. Emmer, M. Versluis, N. De Jong, S. Hilgenfeldt, D. Lohse // The Journal of the Acoustical Society of America. — 2005. — Vol. 118, no. 6. — P. 3499–3505.
14. Estimating the shell parameters of SonoVue® microbubbles using light scattering / J. Tu, J. Guan, Y. Qiu, T. J. Matula // The Journal of the Acoustical Society of America. — 2009. — Vol. 126, no. 6. — P. 2954–2962.
15. *Keller J. B.*, *Miksis M.* Bubble oscillations of large amplitude // The Journal of the Acoustical Society of America. — 1980. — Vol. 68, no. 2. — P. 628–633.

16. Bjerknes forces between small cavitation bubbles in a strong acoustic field / R. Mettin, I. Akhatov, U. Parlitz, C. Ohl, W. Lauterborn // Physical review E. — 1997. — Vol. 56, no. 3. — P. 2924.

17. *Takahira H.*, *Yamane S.*, *Akamatsu T.* Nonlinear oscillations of a cluster of bubbles in a sound field: Bifurcation structure // JSME International Journal Series B Fluids and Thermal Engineering. — 1995. — Vol. 38, no. 3. — P. 432–439.

18. *Ida M.* Phase properties and interaction force of acoustically interacting bubbles: A complementary study of the transition frequency // Physics of fluids. — 2005. — Vol. 17, no. 9. — P. 097107.

19. Secondary Bjerknes forces between two bubbles and the phenomenon of acoustic streamers / N. A. Pelekasis, A. Gaki, A. Doinikov, J. A. Tsamopoulos // Journal of Fluid Mechanics. — 2004. — Vol. 500. — P. 313–347.

20. Effects of coupling, bubble size, and spatial arrangement on chaotic dynamics of microbubble cluster in ultrasonic fields / F. Dzaharudin, S. A. Suslov, R. Manasseh, A. Ooi // The Journal of the Acoustical Society of America. — 2013. — Vol. 134, no. 5. — P. 3425–3434.

21. *Hodgkin A. L.*, *Huxley A. F.* A quantitative description of membrane current and its application to conduction and excitation in nerve // The Journal of physiology. — 1952. — Vol. 117, no. 4. — P. 500.

22. *Hindmarsh J. L.*, *Rose R.* A model of neuronal bursting using three coupled first order differential equations // Proceedings of the Royal society of London. Series B. Biological sciences. — 1984. — Vol. 221, no. 1222. — P. 87–102.

23. *Coombes S.*, *Bressloff P. C.* Bursting: the genesis of rhythm in the nervous system. — World Scientific, 2005.

24. Bioelectronic modulation of carotid sinus nerve activity in the rat: a potential therapeutic approach for type 2 diabetes / J. F. Sacramento, D. J. Chew, B. F. Melo, M. Donegá, W. Dopson, M. P. Guarino, A. Robinson, J. Prieto-Lloret, S. Patel, B. J. Holinski, [et al.] // Diabetologia. — 2018. — Vol. 61. — P. 700–710.

25. *Rössler O. E.* An equation for hyperchaos // Physics Letters A. — 1979. — Vol. 71, no. 2/3. — P. 155–157.

26. *Baier G.*, *Klein M.* Maximum hyperchaos in generalized Hénon maps // Physics Letters A. — 1990. — Vol. 151, no. 6/7. — P. 281–284.

27. *Baier G.*, *Sahle S.* Design of hyperchaotic flows // Physical Review E. — 1995. — Vol. 51, no. 4. — R2712.

28. *Stefański K.* Modelling chaos and hyperchaos with 3-D maps // Chaos, Solitons & Fractals. — 1998. — Vol. 9, no. 1/2. — P. 83–93.

29. *Matsumoto T.*, *Chua L. O.*, *Kobayashi K.* Hyper chaos: laboratory experiment and numerical confirmation // IEEE Transactions on Circuits and Systems. — 1986. — Vol. 33, no. 11. — P. 1143–1147.

30. *Stoop R.*, *Meier P.* Evaluation of Lyapunov exponents and scaling functions from time series // JOSA B. — 1988. — Vol. 5, no. 5. — P. 1037–1045.

31. A p-Ge semiconductor experiment showing chaos and hyperchaos / R. Stoop, J. Peinke, J. Parisi, B. Röhricht, R. Huebener // Physica D: Nonlinear Phenomena. — 1989. — Vol. 35, no. 3. — P. 425–435.

32. Hyperchaotic attractors of three-dimensional maps and scenarios of their appearance / A. Shykhmamedov, E. Karatetskaia, A. Kazakov, N. Stankevich // arXiv preprint arXiv:2012.05099. — 2020.

33. *Pikovsky A.*, *Rosenblum M.*, *Kurths J.* Synchronization: A Universal Concept in Nonlinear Sciences. — Cambridge University Press, 2001. — (Cambridge Nonlinear Science Series).

34. Bifurcation structure of bubble oscillators / U. Parlitz, V. Englisch, C. Scheffczyk, W. Lauterborn // The Journal of the Acoustical Society of America. — 1990. — Vol. 88, no. 2. — P. 1061–1077.

35. Nonlinear transitions of a spherical cavitation bubble / S. Behnia, A. Jafari, W. Soltanpoor, O. Jahanbakhsh // Chaos, Solitons & Fractals. — 2009. — Vol. 41, no. 2. — P. 818–828.

36. *Carroll J. M.*, *Calvisi M. L.*, *Lauderbaugh L. K.* Dynamical analysis of the nonlinear response of ultrasound contrast agent microbubbles // The Journal of the Acoustical Society of America. — 2013. — Vol. 133, no. 5. — P. 2641–2649.

37. *Macdonald C.*, *Gomatam J.* Chaotic dynamics of microbubbles in ultrasonic fields // Proceedings of the Institution of Mechanical Engineers, Part C: Journal of Mechanical Engineering Science. — 2006. — Vol. 220, no. 3. — P. 333–343.

38. Study of encapsulated microbubble cluster based on association schemes perspective / S. Behnia, M. Yahyavi, R. Habibpourbisafar, F. Mottaghi // Ultrasonics Sonochemistry. — 2019. — Vol. 52. — P. 131–141.

39. *Shilnikov A.*, *Kolomiets M.* Methods of the qualitative theory for the Hindmarsh–Rose model: A case study–a tutorial // International Journal of Bifurcation and chaos. — 2008. — Vol. 18, no. 08. — P. 2141–2168.

40. Macro-and micro-chaotic structures in the Hindmarsh-Rose model of bursting neurons / R. Barrio, M. Angeles Martínez, S. Serrano, A. Shilnikov // Chaos: An Interdisciplinary Journal of Nonlinear Science. — 2014. — Vol. 24, no. 2. — P. 023128.

41. *Malashchenko T.*, *Shilnikov A.*, *Cymbalyuk G.* Six types of multistability in a neuronal model based on slow calcium current // PLoS One. — 2011. — Vol. 6, no. 7. — e21782.

42. Dynamical phases of the Hindmarsh-Rose neuronal model: Studies of the transition from bursting to spiking chaos / G. Innocenti, A. Morelli, R. Genesio, A. Torcini // Chaos: An Interdisciplinary Journal of Nonlinear Science. — 2007. — Vol. 17, no. 4. — P. 043128.

43. Spike-train bifurcation scaling in two coupled chaotic neurons / R. Huerta, M. I. Rabinovich, H. D. Abarbanel, M. Bazhenov // Physical review E. — 1997. — Vol. 55, no. 3. — R2108.

44. *Erichsen Jr R.*, *Brunnet L.* Multistability in networks of Hindmarsh-Rose neurons // Physical Review E. — 2008. — Vol. 78, no. 6. — P. 061917.

45. *Yu H.*, *Peng J.* Chaotic synchronization and control in nonlinear-coupled Hindmarsh–Rose neural systems // Chaos, Solitons & Fractals. — 2006. — Vol. 29, no. 2. — P. 342–348.

46. *Etémé A. S.*, *Tabi C. B.*, *Mohamadou A.* Synchronized nonlinear patterns in electrically coupled Hindmarsh–Rose neural networks with long-range diffusive interactions // Chaos, Solitons & Fractals. — 2017. — Vol. 104. — P. 813–826.

47. *Etémé A. S.*, *Tabi C. B.*, *Mohamadou A.* Long-range patterns in Hindmarsh–Rose networks // Communications in Nonlinear Science and Numerical Simulation. — 2017. — Vol. 43. — P. 211–219.

48. *Tamaševičius A.*, *Namajūnas A.*, *Čenys A.* Simple 4D chaotic oscillator // Electronics Letters. — 1996. — Vol. 32, no. 11. — P. 957.

49. *Harrison M. A.*, *Lai Y.-C.* Route to high-dimensional chaos // Physical Review E. — 1999. — Vol. 59, no. 4. — R3799.

50. Chaos-hyperchaos transition / T. Kapitaniak, K.-E. Thylwe, I. Cohen, J. Wojewoda // Chaos, Solitons & Fractals. — 1995. — Vol. 5, no. 10. — P. 2003–2011.

51. *Kapitaniak T.*, *Maistrenko Y.*, *Popovych S.* Chaos-hyperchaos transition // Physical Review E. — 2000. — Vol. 62, no. 2. — P. 1972.

52. *Yanchuk S.*, *Kapitaniak T.* Chaos–hyperchaos transition in coupled Rössler systems // Physics Letters A. — 2001. — Vol. 290, no. 3/4. — P. 139–144.

53. Three-dimensional Hénon-like maps and wild Lorenz-like attractors / S. V. Gonchenko, I. Ovsyannikov, C. Simó, D. Turaev // International Journal of Bifurcation and Chaos. — 2005. — Vol. 15, no. 11. — P. 3493–3508.

54. Towards scenarios of chaos appearance in three-dimensional maps / A. Khokhlov, N. Brilliantov, S. Belyakin, A. Dzhanoev, E. Zhuchkova, O. Kotlyarov, S. Krotov, S. Larionov, E. Postnikov, G. Riznichenko, [et al.] // Rus. J. Nonlin. Dyn. — 2012. — Vol. 8, no. 1. — P. 3–28.

55. Simple scenarios of onset of chaos in three-dimensional maps / A. Gonchenko, S. Gonchenko, A. Kazakov, D. Turaev // International Journal of Bifurcation and Chaos. — 2014. — Vol. 24, no. 08. — P. 1440005.

56. Methods of Qualitative Theory in Nonlinear Dynamics. Part I . / L. Shilnikov, A. Shilnikov, D. Turaev, L. Chua. — 1998.

57. Hidden attractors in dynamical systems / D. Dudkowski, S. Jafari, T. Kapitaniak, N. V. Kuznetsov, G. A. Leonov, A. Prasad // Physics Reports. — 2016. — Vol. 637. — P. 1–50.

58. *Trefethen L.*, *Bau D.* Numerical Linear Algebra: Twenty-Fifth Anniversary Edition. — SIAM, Society for Industrial, Applied Mathematics, 2022. — (Other Titles in Applied Mathematics).

59. Lyapunov characteristic exponents for smooth dynamical systems and for Hamiltonian systems; a method for computing all of them. Part 1: Theory / G. Benettin, L. Galgani, A. Giorgilli, J.-M. Strelcyn // Meccanica. — 1980. — Vol. 15. — P. 9–20.

60. *Oseledec V. I.* A multiplicative ergodic theorem, Lyapunov characteristic numbers for dynamical systems // Transactions of the Moscow Mathematical Society. — 1968. — Vol. 19. — P. 197–231.

61. *Ashwin P.*, *Buescu J.*, *Stewart I.* Bubbling of attractors and synchronisation of chaotic oscillators // Physics Letters A. — 1994. — Vol. 193, no. 2. — P. 126–139.

62. *Ashwin P.*, *Buescu J.*, *Stewart I.* From attractor to chaotic saddle: a tale of transverse instability // Nonlinearity. — 1996. — Vol. 9, no. 3. — P. 703.

63. *Saha A.*, *Feudel U.* Extreme events in FitzHugh-Nagumo oscillators coupled with two time delays // Physical Review E. — 2017. — Vol. 95, no. 6. — P. 062219.

64. Secondary Bjerknes forces between two bubbles and the phenomenon of acoustic streamers / N. A. Pelekasis, A. Gaki, A. Doinikov, J. A. Tsamopoulos // Journal of Fluid Mechanics. — 2004. — Vol. 500. — P. 313–347.

65. *Gonchenko A. S.*, *Gonchenko S.* Variety of strange pseudohyperbolic attractors in three-dimensional generalized Hénon maps // Physica D: Nonlinear Phenomena. — 2016. — Vol. 337. — P. 43–57.

66. *Borisov A. V.*, *Kazakov A. O.*, *Sataev I. R.* Spiral chaos in the nonholonomic model of a Chaplygin top // Regular and Chaotic Dynamics. — 2016. — Vol. 21. — P. 939–954.

67. Chaotic dynamics and multistability in the nonholonomic model of a Celtic stone / A. S. Gonchenko, S. V. Gonchenko, A. O. Kazakov, E. A. Samylina // Radiophysics and Quantum Electronics. — 2019. — Vol. 61. — P. 773–786.

68. *Izhikevich E. M.* Dynamical systems in neuroscience. — MIT press, 2007.

69. Bursts as a unit of neural information: selective communication via resonance / E. M. Izhikevich, N. S. Desai, E. C. Walcott, F. C. Hoppensteadt // Trends in neurosciences. — 2003. — Vol. 26, no. 3. — P. 161–167.

70. *Lisman J. E.* Bursts as a unit of neural information: making unreliable synapses reliable // Trends in neurosciences. — 1997. — Vol. 20, no. 1. — P. 38–43.